

Early Science Result from the Japanese Virtual Observatory: AGN and Galaxy Clustering at $z = 0.3$ to 3.0 *

Yuji SHIRASAKI¹ Masahiro TANAKA¹ Masatoshi OHISHI¹ Yoshihiko MIZUMOTO¹ Naoki YASUDA² Tadafumi TAKATA¹

¹National Astronomical Observatory of Japan, 2-21-1 Osawa, Mitaka City, Tokyo, 181-8588, Japan

²Institute for the Physics and Mathematics of the Universe Library, The University of Tokyo, 5-1-5 Kashiwa-no-ha, Kashiwa, Chiba, Japan
yuji.shirasaki@nao.ac.jp

(Received 2009 0; accepted 2009 0)

Abstract

We present the result of projected cross correlation analysis of AGNs and galaxies at redshifts from 0.3 to 3.0. The Japanese Virtual Observatory (JVO) was used to obtain the Subaru Suprime-Cam images and UKIDSS catalog data around AGNs. We investigated 1,809 AGNs, which is about ten times larger a sample than that used in previous studies at redshifts larger than 0.6. We found significant excess of galaxies around the AGNs at redshifts from 0.3 to 1.8. For the low redshift samples ($z < 0.9$), we obtained correlation length of $r_0 = 5\text{--}6\text{ h}^{-1}\text{Mpc}$ ($\gamma = 1.8$), which indicates that the AGNs at this redshift range reside in a similar environment around typical local galaxies. We also found that AGNs at higher redshift ranges reside in a denser environment than lower redshift AGNs; For $z = 1.3 \sim 1.8$ AGNs, the cross correlation length was measured as $11_{-3}^{+6}\text{ h}^{-1}\text{Mpc}$ ($\gamma = 1.8$). Considering that our galaxies sample is based on optical observations with Suprime-Cam at the redshift range, it is expected that blue star-forming galaxies are dominant constituents of the clustering. It is successfully demonstrated that the use of the archive through the Virtual Observatory system can provide a powerful tool for investigating the small scale environment of the intermediate redshift AGNs.

Key words: astronomical data bases: miscellaneous — galaxies: clusters: general — galaxies: nuclei — cosmology: large-scale structure of universe

1. Introduction

It has been believed that the origin of AGN activity is accretion of matter into a massive black hole at the center of a galaxy, and that almost all massive galaxies have such a black hole (e.g. Salpeter 1964; Lynden-Bell 1969; Rees 1984; Kormendy & Richstone 1995; Richstone et al. 1998). In order to explain the activity of the AGNs with mass $\sim 10^9\text{ M}_\odot$, a large fraction of matter in the galaxy must be delivered to the inner region of the galaxy on a short timescale, $\ll 10^9\text{ yr}$ (Hopkins et al. 2008). One possible mechanism for causing rapid gas inflows toward the central region would be a major galaxy merger between gas-rich galaxies (e.g. Sanders et al. 1988; Barnes & Hernquist 1991; Barnes & Hernquist 1996; Kauffmann and Haehnelt 2000; Granato et al. 2004; Springel et al. 2005; Croton et al. 2006). If this is the case, AGNs are expected to be found in an environment ¹ of higher density than typical galaxies since the merger occurs more frequently at a higher density region.

There is some observational evidence that mass assembly of a larger system terminates earlier than that of a

smaller system (e.g. Cowie et al. 1996; Kodama et al. 2004). From these observational facts, it is expected that at higher redshift the merger occurs in an environment with high galaxy density. Thus the AGNs produced at the higher redshift should be observed in a more crowded region.

Measurements of the two-point correlation function of optically selected QSOs were performed by using the large dataset of QSOs obtained by 2dF and SDSS surveys (Croom et al. 2005; Ross et al. 2009; Shen et al. 2009; Myers et al. 2006; Myers et al. 2007). Ross et al. (2009) measured the real-space correlation lengths for $z = 0.3\text{--}2.2$ QSO, which was in the range of $6\text{--}11\text{ h}^{-1}\text{Mpc}$ for fixed power index of $\gamma = 2.0$. Shen et al. (2009) analyzed data of QSOs at higher redshifts and obtained the real-space correlation lengths of $14.58 \pm 2.7\text{ h}^{-1}\text{Mpc}$ ($\gamma = 2.0$) and $21.04 \pm 3.39\text{ h}^{-1}\text{Mpc}$ ($\gamma = 2.0$) at $z = 2.9\text{--}3.5$ and $z = 3.5\text{--}5.0$, respectively.

The correlation length of the local quiescent galaxy has been measured by many authors (e.g. Brown et al. 2000; Norberg et al. 2002; Budavari et al. 2003; Madgwick et al. 2003; Hawkins et al. 2003; Zehavi et al. 2005; Ma et al. 2009). Zehavi et al. (2005) measured real-space correlation length and obtained $5.59 \pm 0.11\text{ h}^{-1}\text{Mpc}$ for flux-limited sample with $14.5 < r < 17.77$ and $-22 < M_r < -19$ (for $h = 1$). Thus the large scale environment of QSOs is almost equivalent to or only slightly larger than the environment of typical local galaxies at redshift less than 2.2,

* Based on data collected at Subaru Telescope, which is operated by the National Astronomical Observatory of Japan (NAOJ). Data is retrieved from the JVO (<http://jvo.nao.ac.jp/portal>) operated by NAOJ.

¹ The term of environment is used to represent the excess number density around the region relative to the average at the redshift.

and at higher redshift the galaxy number density around the QSOs increases with the redshift.

The direct measurement of QSO two-point correlation function requires a large number of QSO samples and large sky coverage, thus only the large survey projects such as 2dF and SDSS can provide a precise and reliable measurement. The measurement of QSO-galaxy cross correlation function, on the other hand, provides a direct insight on the local environment of QSO with fewer samples, although it is limited to lower redshifts where spectroscopic observation of galaxies is feasible.

A lot of studies have been made to investigate the relation of QSO/AGN environment with a type and luminosity of the AGNs and their evolution with redshift (e.g. Miller et al. 2003; Sorrentino et al. 2006; Coldwell and Lambas 2006; Serber et al. 2006; Strand et al. 2008; Barr et al. 2003; Coil et al. 2007; Adelberger and Steidel 2005; Bornancini et al. 2007).

Studies of the environment around optically selected AGNs at redshift < 0.6 have been carried out by many authors by using the SDSS data. Miller et al. (2003) estimated the fraction of galaxies associated with an AGN, based on 4921 galaxies with redshift less than ~ 0.1 . They found that the fraction of galaxies associated with an AGN is independent of density of local galaxy. Sorrentino et al. (2006) examined 1829 AGNs at redshift < 0.1 , and found no evidence of a relation between the density of local galaxy and the AGN activity. Coldwell and Lambas (2006) analyzed the environment of ~ 2000 AGNs at redshift < 0.2 , and found that the number density of galaxies around the AGNs is similar to that of a typical galaxy.

Although these results show that the optically selected AGNs do not reside in an area of high overdensity, there are several studies which indicate the small-scale overdensity around the AGNs.

Serber et al. (2006) analyzed small-scale environment of 2,028 $z < 0.4$ SDSS QSOs and found that the QSOs are located in higher density region than are L^* galaxies and the over-density increases with decreasing scale at a distance of less than $0.5h^{-1}\text{Mpc}$ of the QSO. They also reported that there is a luminosity dependence of the density enhancement at the small-scale and the brightest end. Strand et al. (2008) also investigated the relationship of the AGN environment to type (type I, type II), luminosity and redshift of the AGN at small distance less than $2h^{-1}\text{Mpc}$. They extended the redshift range up-to 0.6 compared to the work of Serber et al. (2006) by applying a photometric redshift cut in their selection of galaxies to reduce the projection effect. The number of AGN samples was increased to ~ 11000 . They concluded that the AGN environment depends on the luminosity of AGNs but not on the type of AGNs, and that there is marginal evidence on variation of its environment around type I QSOs as a function of redshift.

Since the observation of galaxies by the SDSS is limited to the redshift of less than ~ 0.6 , measurements of AGN environment at higher redshifts need to be carried out by an infrared instrument on a 2–4 m class telescope or optical and/or near infrared observations by 8–10 m class

telescopes.

Coil et al. (2007) measured clustering properties around 52 SDSS and DEEP2 QSOs at redshifts 0.7 – 1.4, by cross-correlating each QSO with DEEP2 galaxies. They found that the clustering scale length between the QSOs and galaxies is comparable to that obtained by auto-correlation of DEEP2 galaxies, and obtained the correlation length of $3.3 \pm 0.7h^{-1}\text{Mpc}$. They found no significant dependence on luminosity nor redshift. Adelberger and Steidel (2005) examined clustering property of 79 AGNs with absolute magnitude from -30 to -20 at redshifts from 1.5 to 3.5, by cross correlating with the 1627 galaxies with measured redshift. The galaxy sample used in their analysis was constituted of color-selected spectroscopic targets. They divided 79 AGNs into two luminosity groups, and derived correlation lengths of $4.7 \pm 2.3h^{-1}\text{Mpc}$ and $5.4 \pm 1.2h^{-1}\text{Mpc}$ for the low and high luminosity groups, respectively. They reported no evidence of luminosity dependence. Bornancini et al. (2007) examined the correlation between the SDSS QSOs and distant red galaxies (DRG) at redshifts from 1 to 2, and obtained correlation length of $5.4 \pm 1.6h^{-1}\text{Mpc}$.

All of these results for high redshift ($z = 0.7\text{--}3.5$) AGN/QSOs also show no significant over density of their environment. Although the optically selected AGNs/QSOs seem to be located in an environment comparable to that of local typical galaxies as introduced above, there have been some studies which report some types of QSOs such as radio-loud QSOs and X-ray selected AGNs are associated with a higher density region.

Barr et al. (2003) observed environments of 21 radio-loud QSOs at $0.6 < z < 1.1$ with multiple filters of optical to near infrared bands. The observation showed that the radio-loud QSOs at this redshift range exist in a wide variety of environment (field galaxies, compact groups, and rich clusters), and indicated no evidence of redshift dependence of the environment. They also found that the QSOs are not always located at the center of a galaxy group or cluster, which contrast with low redshift clusters where QSOs are located at the center of galaxy distribution. Enoki et al. (2003) predicted that, at redshift from 1 to 2, QSOs are located in various environments from small groups of galaxies to clusters of galaxies based on a semi-analytic model of galaxy and QSO formation. This prediction is consistent with the observational evidence obtained by Barr et al. (2003). The over density around the radio-loud QSOs were also reported by some other authors (e.g. Yee & Green 1984; Yee & Green 1987; Ellingson et al. 1991; Hutchings et al. 1999; Kauffman et al. 2008).

In contrast, several studies reported that the environment of the radio-loud and radio-quiet QSOs were indistinguishable (e.g. Fisher et al. 1996; Wold et al. 2001; McLure & Dunlop 2001), though the number of samples used by these authors was not so large as several tens of samples.

There have been a lot of studies on the environment of the X-ray selected AGNs (e.g. Mullis et al. 2004; Grazian et al. 2004; Gilli et al. 2005; Yang et al. 2006; Miyaji et al. 2007; Hickox et al. 2009; Gilli et al. 2009; Krumpke et al.

2010; Coil et al. 2009).

Hickox et al. (2009) examined the environment of AGN selected from radio observations with Weterbork Synthesis Radio Telescope, X-ray observations of Chandra XBootes Survey, and mid-IR observations of Spitzer IRAC Shallow Survey. They measured cross-correlation between these AGNs and galaxies on scales of $0.3\text{--}10\text{ h}^{-1}\text{Mpc}$ and derived the correlation length of 6.3 ± 0.6 ($\gamma = 1.8\pm0.2$), 4.7 ± 0.3 ($\gamma = 1.6\pm0.1$), and $3.7\pm0.4\text{ h}^{-1}\text{Mpc}$ ($\gamma = 1.5\pm0.1$) for AGNs selected in radio, X-ray, and infrared band. They concluded that the X-ray selected AGNs were clustered similar to typical galaxies, less clustered than radio AGNs, and more clustered than IR AGNs.

Krumpe et al. (2010) examined the environment of X-ray selected AGNs, by using cross correlation measurement between ~ 1550 ROSAT broad-line AGN and $\sim 46,000$ luminous red galaxies (LRGs) at $z = 0.16\text{--}0.36$. They obtained real space correlation length of $6.93^{+0.27}_{-0.28}\text{h}^{-1}\text{Mpc}$ for the AGNs and LRGs, and also estimated the AGN auto correlation length of $4.3^{+0.4}_{-0.5}\text{h}^{-1}\text{Mpc}$. They also measured an X-ray luminosity dependence of the clustering and concluded that low luminosity samples have a correlation length similar to that of blue star-forming galaxies at low redshift, and high luminosity samples have a larger correlation length than the lower luminosity samples and is consistent with the clustering of red galaxies.

The other studies which measured auto correlation of X-ray selected AGNs from ROSAT all sky survey by Mullis et al. (2004) and Grazian et al. (2004), from Chandra Deep Field North and South by Gilli et al. (2005) and Yang et al. (2006), from XMM-COSMOS field by Gilli et al. (2009) and Miyaji et al. (2007), and from AEGIS field by Coil et al. (2009). They obtained auto-correlation lengths of $6\text{--}10\text{h}^{-1}\text{Mpc}$ for the X-ray selected AGNs. These results are slightly larger than typical local galaxies and quite similar to the optically selected SDSS QSOs.

Although the observations of AGN-galaxies clustering up to redshift ~ 2.0 indicate that AGNs do not reside in a particularly high density environment, QSO-QSO clustering study indicates that the environment of AGN at higher redshift is more crowded than in the low redshift Universe. Considering that the number density of bright AGNs peaks around redshift ~ 2 (Ueda et al. 2003; Richards et al. 2006), it is important to extend the study of AGN environment up to redshift 2 and beyond to solve the mechanism of co-evolution of AGNs and galaxies.

In this paper we present the result on measurements of AGN environment at redshifts from 0.3 to 3.0 , which is the first scientific result obtained from the Japanese Virtual Observatory (JVO). The reduced Subaru Suprime-Cam images are open to public through the JVO system. The JVO portal provides a functionality to search for multiple regions from its image data service by issuing a single JVOQL, which is an extension of database language SQL and can describe a coordinate join between the Suprime-Cam image metadata table and a QSO/AGN catalog table. The UKIDSS World DR2 is also used to detect galax-

ies which are dark in optical bands but bright enough to be detected in near-infrared bands. The total number of QSO/AGN samples used in this work is ~ 1809 , and $\sim 90\%$ of the QSO/AGN samples comes from the SDSS and 2dF QSO catalog. Note that this work uses the largest sample with deep optical images, which are typically deeper than 24 mag . By using the deep optical images, we can also measure the clustering property of faint and blue star forming galaxies around AGNs at high redshift ($z \sim 1\text{--}2$), which have not been well explored by any other studies. Note also that our work would be free from the cosmic variance, since the AGNs we have used are distributed through a wide area of the sky.

Throughout this paper, we assume a cosmology with $\Omega_m = 0.3$, $\Omega_\lambda = 0.7$ and $h = 0.7$. All magnitudes are given in the AB system. All the distances are measured in comoving coordinates. The correlation length is presented in unit of h^{-1}Mpc .

2. The Datasets

All the data used in this work were obtained from the Japanese Virtual Observatory (JVO) portal (<http://jvo.nao.ac.jp/portal>). The dataset downloaded through the JVO portal is: Catalog of Quasars and Active Galactic Nuclei (12th Ed.) by Veron-Cetty et al. (2006), SDSS DR-5 Quasar Catalog (4th Ed.) by Schneider et al. (2007), Subaru Suprime-Cam reduced images (version 0.1.24) of the JVO Subaru archive, and UKIDSS DR2 catalog by Warren et al. (2007). Now we describe the procedure for selecting data in order to achieve our research objectives.

First we searched for AGNs observed with the Suprime-Cam or the UKIDSS survey at the redshift range of $0.3\text{--}3.0$. We selected AGNs whose K-corrected absolute V band magnitude was in the range from -30 to -20 . The K correction was made by assuming power law index of $\alpha = -0.5$ for AGN spectrum and calculated as $k = -2.5(\alpha + 1)\log(1 + z)$. Then we removed AGNs that were located near another lower redshift AGN within an angular distance corresponding to 8 Mpc at the AGNs' redshift. This filtering aimed to reduce the projection effect of galaxy clustering associated with other nearby AGNs.

For each AGN among these samples, the Suprime-Cam images of B, V, Rc, Ic, i', and z' band and the UKIDSS K-band data were retrieved, and uniformity of the images and data coverage for the AGN field were examined.

The quality of some of the Suprime-Cam images retrieved from the JVO is highly inhomogeneous, because the images were created by stacking all the frames. Certain parts of an image, therefore, may have significantly shorter exposure time than other parts. The inhomogeneity was estimated from the distribution of root mean squares (RMS) of the background noise, which was calculated by the SExtractor (Bertin and Arnouts 1996) at every image pixel. We removed images where the standard deviation of RMS over the entire AGN field was larger than 10% of the average. The Suprime-Cam im-

ages which were not associated with photometric calibration data were not used in this analysis either.

Since we were interested especially in an environment of high redshift ($z > 1$) AGN, we masked bright and extended sources on the Suprime-Cam images, so that low redshift bright galaxies were effectively filtered from our galaxy sample. The masked regions were defined as a region where more than 100 contiguous pixels were illuminated with a flux higher than 10 sigma of the background fluctuation. Comparing with an unmasked image, we estimated that the masked sources were about two magnitudes brighter than the peak of the magnitude distribution, which was ~ 22 mag on average. Object catalogs for Suprime-Cam images were created separately for each observation band using the SExtractor (Bertin and Arnouts 1996).

In order to examine the data coverage of the AGN field, an effective observation area was calculated for each annulus centered on an AGN location, which has a corresponding width of 0.1 Mpc. The effective area observed with the Suprime-Cam was calculated by counting the unmasked pixels of the image. The coverage of the UKIDSS data was estimated from a fraction of an area where number density of objects was lower than the average at the same annulus by five sigma.

It is difficult, however, to measure the coverage fraction of the annulus for which the expected source number is too small to measure the density variation in the annulus. To evaluate the coverage of the low count annulus, we estimated the average number density expected for full coverage, and compared the observed number in the annulus with the expected number. The average number density was estimated from the annulus with second largest density among the top-five annuli in terms of the number of detected sources. If the observed number is below the expected number by five sigma, we considered the annulus to be an unobserved area, that is 0% of coverage.

We set a threshold on the data where at least 80% of every annulus should be observed. The data that did not meet this threshold were removed. The fraction of data coverage estimated as described above was used in the calculation of number density of galaxy at each annulus. After these selections, 2689 AGNs were selected for further analysis.

To improve the signal to noise ratio, we removed the data of shallow observations based on the average number density, ρ_0 , of detectable galaxies at the AGN redshift. ρ_0 was estimated by integrating a luminosity function up to an effective limiting magnitude, m_{limit} , of each Suprime-Cam image or UKIDSS data. The detailed description for determination of ρ_0 will be described in the next section.

Then we selected data where ρ_0 was greater than 10^{-5} Mpc^{-3} at any one of the observation bands. The distribution of ρ_0 vs AGN redshift z are shown in figure 1 for data of $\rho_0 > 10^{-7}$. In the figure, ρ_0 is the largest value among all the observation bands for each AGN. One can see a clear separation between the samples which are observed in the UKIDSS Large Area Survey (LAS) (lower cluster of open circles), and the samples observed with the

Suprime-Cam and UKIDSS Deep Extragalactic Survey (DES) (upper cluster of crosses and open circles). We applied the selection criterion of $\rho_0 > 10^{-5} \text{ Mpc}^{-3}$, which limit the maximum redshift of UKIDSS LAS samples to ~ 1.3 . The number of AGN selected with this criterion is 2023.

The foreground cluster or group of galaxies can be a noise for the clustering analysis. To reduce the effect of accidental alignment of the nearby cluster, we calculated a clustering coefficient, B_{QG} , around each AGN, which was defined as $\xi(r) = B_{QG} r^{-\gamma}$, and B_{QG} was calculated as (Barr et al. 2003):

$$B_{QG} = \frac{3 - \gamma}{2\pi} \frac{N_{\text{total}} - N_{bg}}{\rho_0} (1 \text{ Mpc})^{\gamma-3}, \quad (1)$$

where N_{total} is the total number of observed galaxies at $r_p < 1$ Mpc, and N_{bg} is the expected background count at $r_p < 1$ Mpc estimated from the averaged density at $r_{bg, \text{min}} < r_p < r_{bg, \text{max}}$. The distance ranges $r_{bg, \text{min}}$ and $r_{bg, \text{max}}$ were determined for each redshift group, and they are summarized in table 1. If a cluster of galaxies is accidentally located in front of the AGN, significantly large B_{QG} values would be observed. Figure 2 shows the distribution of $\log |B_{QG}|$ for 2023 AGNs which satisfied the ρ_0 criterion. The selection criteria used here were $|B_{QG}| \leq 1 \times 10^4$. Abell class 0 clusters corresponds to $B_{QG} \sim 300 \text{ Mpc}^{1.77}$ (McLure & Dunlop 2001). The upper bound of this selection range corresponds to a cluster which has 30 times larger clustering coefficient than the Abell class 0, and it is expected that B_{QG} of a real system rarely exceeds this criteria. Thus most of the samples rejected with this criteria are the ones with an uncertainty of the clustering coefficient as large as this boundary or clusters accidentally located near the line of sight. Applying both the ρ_0 and B_{QG} criteria, the number of AGNs was reduced to 1976.

It is also possible that the nearby cluster or high density region is located in a region offset from the AGN. To remove such samples, the reduced χ^2 and maximum deviation σ_{max} of radial distribution of galaxy density around the AGN were calculated at distance range of 1 Mpc to $r_{bg, \text{min}}$. The distributions of the reduced χ^2 and maximum deviation σ_{max} for the 1976 AGN samples are shown in figures 3 and 4. The criteria used here were $\chi^2/(n-1) \leq 3.0$ and $\sigma_{\text{max}} \leq 5.0$. After this selection, the total number of AGNs was 1828.

Figure 5 shows the distribution of K-corrected V-band absolute magnitude and redshift of the AGNs selected by the above criteria. Open circles represent AGNs for which the analysis was made using the UKIDSS data, and crosses represent AGNs for which the analysis was made using the Suprime-Cam data. The histograms of AGN redshift for dim AGNs ($M_V \geq -25$) and bright AGNs ($M_V < -25$) are shown in figure 6.

In table 2, the number of AGNs used in this work are shown for each data subset (z1-D to z5-B defined in section 4) and for each origin of the AGN identification. The low redshift and high luminosity AGNs, and high redshift and low luminosity AGNs were not analyzed for their poor

statistics. As a result the total number of analyzed AGNs was reduced to 1809.

The column “SDSS” of the table represents the number of AGNs which are contained in the SDSS QSO catalog (4-th ed.). The column “2dF” represents the number of AGNs which are contained in the 2dF QSO catalog but not contained in the SDSS catalog. The AGNs which are contained in both the SDSS and 2dF catalog are counted as “SDSS”. Among the AGNs which are not contained in the SDSS catalog nor the 2dF catalog, the AGNs which were identified based on an optical, UV, or infrared observations are counted as “UV-OPT-IR”, the AGNs which were selected from X-ray or Radio catalog are counted as “XRAY” or “RADIO”, respectively. About ninety percent of the AGNs are selected from the large survey of SDSS and 2dF, thus our AGN samples are nearly homogeneous and dominated by optically selected AGNs.

The celestial distribution of the 1809 AGNs is shown in figure 7. Since a large fraction of AGNs comes from the SDSS catalog, the distribution almost follows the SDSS survey area. The distribution of the right ascension and the declination are also shown in figure 8 for all the samples (open histogram) and samples which have data of Suprime-Cam (shading histogram). The concentration to declination ~ 0 degree is due to the contribution of UKIDSS LAS survey. The most significant concentration of Suprime-Cam observations is located at the Sextans field (RA = $150^\circ - 157^\circ$, Dec = $-4^\circ - +1^\circ$). The total number of AGNs in the Sextans field is 80, and their number fraction at each subset group is $\sim 20\%$ for z4-B and z5-B group, and less than 6% for the other groups. We confirmed that this concentration to a specific field did not affect the result so much, and it will be discussed in section 5. Although there is a slight concentration to specific fields, the AGNs are distributed in an extended area of the sky, and we can expect that the bias effect (cosmic variance) would be mostly negligible in our analysis.

The Suprime-Cam images provided by the JVO portal were processed using the JVO Suprime-Cam reduction pipeline (version 0.1.24) which was developed based on the Suprime-cam Deep Field REDuction (SDFRED) package (Ouchi et al. 2004). The data reduction was carried out on the JVO grid computing system (Shirasaki et al. 2008). All the data obtained before December 2006 were used to create mosaic images. The SDFRED is based on a software package developed for Suprime-Cam data reduction (Yagi et al. 2002).

The data were reduced in the following procedure for each CCD frame: 1) bias subtraction; 2) flat field correction; 3) distortion correction; and 4) astrometric correction. The positions, rotation angles, and flux normalization factors relative to a reference frame were calculated for every frame, then they were stacked to make a single mosaic image. The photometry was performed using the data of standard star observations which were taken on the day that one of the stacked frames were observed. The comparison with the SDSS catalog shows the differences of photometric magnitudes were less than 0.2 for 90% of the data compared. The astrometric accuracy was esti-

mated by comparing with the USNO catalog. The peak of the distribution of angular difference from the USNO data was 0.3 arcsec, and the difference was less than 1.2 arcsecond for 99% of the analysed data.

3. Estimation of ρ_0

Estimation of ρ_0 , which is an average number density of observed galaxy at AGN redshift, is crucial for determining the cross correlation length of AGNs and galaxies. Since redshift of galaxy is not measured in this work, ρ_0 cannot be determined directly from the data used here. Therefore, it needs to be indirectly derived by model calculation under reasonable assumptions.

The luminosity function of galaxy $\phi(M)$ is one of the functions required for the model calculation. Only the observable that can be used to infer the density of observed galaxy is an observed magnitude distribution $N(m)$. The observed magnitude distribution is a product of true magnitude distribution $N_{\text{true}}(m)$ and detection efficiency $DE(m)$ for an object of apparent brightness m . Once the model functions for $\phi(M)$, $N_{\text{true}}(m)$ and $DE(m)$ are derived, we can estimate ρ_0 by comparing the observable $N(m)$ with the model prediction.

A brief procedure for determining ρ_0 and its uncertainty is described as follows; we define a parameter m_{limit} which is closely related with the limiting magnitude of observation and is used to calculate ρ_0 by integrating the luminosity function $\phi(M)$ to the corresponding absolute magnitude at the AGN redshift. We estimate m_{limit} under the assumption that the cumulative fraction of apparent magnitude above m_{peak} has a constant value of F_{limit} at m_{limit} . This assumption would be valid if the observations were carried out under identical conditions. This is, however, not actually the case, and F_{limit} is not a constant but a variable depending on the observational condition. Thus we calculated the expected value of F_{limit} for each observation of AGN field, and we considered the most frequent value of F_{limit} to be an estimator for the most probable value of ρ_0 , and the lower and upper limit to F_{limit} to be an estimator for uncertainty of ρ_0 .

First we describe the model of luminosity function used in this work. We parametrized the luminosity function of galaxy by means of the absolute magnitude M , redshift z , and source frame wavelength λ by using the luminosity functions obtained by Gabasch et al. (2004) for 1500Å, 2800Å, u, B and g' bands, Gabasch et al. (2006) for r', i', and z' bands, and Cirasuolo et al. (2007) for K band. The parameters α , ϕ_0 , and M_0 of the Schechter function for each rest-frame wavelength band were parametrized by a polynomial function of redshift. Then, for each redshift, these parameters were represented as a function of rest-frame wavelength by interpolating with the cubic spline. Using this parametrization, we obtained luminosity function $\phi(M; z, \lambda)$ for an arbitrary redshift and rest-frame wavelength.

ρ_0 is calculated by integrating the product of the luminosity function $\phi(M; z, \lambda)$ and detection efficiency $DE(M + DM)$ for a source with absolute brightness of

M (apparent brightness $m = M + DM$) at AGN redshift z . DM is a distance modulus for redshift z . For simplicity, we use an effective limiting magnitude m_{limit} as a characteristic parameter for $DE(m)$. m_{limit} is defined so that the integral of luminosity function up to $m_{\text{limit}} - DM$ equals to ρ_0 :

$$\rho_0 = \int_{m_{\text{low}} - DM}^{\infty} \phi(M) DE(M + DM) dM = \int_{m_{\text{low}} - DM}^{m_{\text{limit}} - DM} \phi(M) dM, \quad (2)$$

where m_{low} is a lower boundary of the apparent magnitude for the integration.

The luminosity functions were evaluated for the AGN redshift and for the rest frame wavelength corresponding to the center wavelength of the observation band. We assumed the following function for modeling the detection efficiency :

$$DE(m) = \begin{cases} 1 & (m < m_{\text{th}}) \\ \exp(-(m - m_{\text{th}})^2 / \sigma_m^2) & (m \geq m_{\text{th}}), \end{cases} \quad (3)$$

where m_{th} and σ_m represent the magnitude where detection efficiency starts to decrease and the attenuation width of the detection efficiency, respectively. In the case of Suprime-Cam data, the detection efficiency rapidly decreases at the bright magnitude side owing to the masking procedure described in the previous section. This effect was approximated by introducing the lower cut-off magnitude m_{low} . m_{low} is a minimum of the observed magnitude excluding the first 5% of all the sources ordered with their magnitudes. The number density at the bright end of the luminosity function is small and the error on the ρ_0 estimation is expected to be lower than a few %, which is negligible compared to the error caused from the uncertainty of m_{limit} .

The only observable that can be used to determine m_{limit} is the observed magnitude distribution $N(m)$. Especially, the distribution beyond the peak magnitude m_{peak} can be a sensitive estimator for m_{limit} . Thus we define the cumulative fraction $F(m)$ to estimate m_{limit} as follows:

$$F(m) = \int_{m_{\text{peak}}}^m N(m') dm' / \int_{m_{\text{peak}}}^{\infty} N(m') dm'. \quad (4)$$

To calculate a model function for $F(m)$, we need a model function for *true* magnitude distribution $N_{\text{true}}(m)$. We assumed a broken power law function for $N_{\text{true}}(m)$:

$$N_{\text{true}}(m) = \begin{cases} c \cdot 10^{a(m - m_b)} & (m < m_b) \\ c \cdot 10^{b(m - m_b)} & (m \geq m_b), \end{cases} \quad (5)$$

where m_b is a break magnitude of the magnitude distribution. Using this model function, the observed magnitude distribution can be calculated as $N_{\text{model}}(m) = N_{\text{true}}(m) \times DE(m)$. Applying this to the equation (4), we can obtain the model function $F_{\text{model}}(m)$.

To show how well the model function $N_{\text{model}}(m)$ describes an actual observed magnitude distribution, the model functions fitted to the observation are shown in figure 9. The fitting results for two examples of UKIDSS K-band (left histogram) and Suprime-Cam R-band (right)

are shown in the figure. The best fit parameters for these examples are: $a = 0.47 \pm 0.02$, $b = 0.20 \pm 0.01$, $m_b = 19.0 \pm 0.1$, $m_{\text{th}} = 20.8 \pm 0.06$ and $\sigma_m = 1.11 \pm 0.03$ for UKIDSS K-band, and $a = 0.98 \pm 0.05$, $b = 0.28 \pm 0.01$, $m_b = 23.4 \pm 0.04$, $m_{\text{th}} = 26.1 \pm 0.02$ and $\sigma_m = 0.51 \pm 0.01$ for Suprime-Cam R-band. The break magnitude m_b approximately corresponds to M_0 of the Schechter function for the maximum observable redshift, thus it is expected to correlate with m_{th} which is a parameter related with sensitivity of the observation. Since an accurate value of m_b is not required for the estimation of m_{limit} , we simply used an empirical relation of $m_b = m_{\text{th}} - 2.5$.

The cumulative fraction at m_{limit} , $F_{\text{limit}} = F(m_{\text{limit}})$, depends on the limiting magnitude of the observation, redshift of the AGN, the observation band, and the model parameter of N_{true} . We, therefore, calculated F_{limit} for various plausible parameter ranges: $z = 0.3 - 3.0$, $\sigma_m = 0.5 - 1.2$, $a = 0.6$, $b = 0.1 - 0.6$, $m_{\text{th}} = 19 - 26$, and $\rho_0 > 10^{-5}$. The last criteria is the same as was applied to the observational data. To choose the ranges of parameters σ_m , b and m_{th} , we fit the magnitude distribution for each AGN sample to the model function $N_{\text{model}}(m)$. Since the statistics of UKIDSS LAS samples were too poor to fit to the model function, we summed every five samples in order from the lowest m_{peak} sample, and fit the model to the summed distribution. The ranges of b , σ_m and m_{th} were determined so that more than 90% of the samples were included. Since the parameter a is insensitive to F_{limit} , it was fixed to an average value of 0.6.

For these parameter ranges, we obtained 0.1, 0.6, and 0.8 for the minimum, median, and maximum values of F_{limit} , respectively. Therefore, we calculated the most probable value of ρ_0 by integrating the luminosity function up to m_{limit} determined with $F_{\text{limit}} = 0.6$, and lower and upper boundary with $F_{\text{limit}} = 0.1$ and 0.8, respectively.

4. Cross-Correlation Analysis

The two-point cross-correlation function, ξ , is generally used to measure the clustering properties between an AGN and its surrounding galaxies. It is defined as:

$$\xi(r) = \rho(r) / \rho_0 - 1, \quad (6)$$

where $\rho(r)$ is the number density of galaxies at a distance r from an AGN, and ρ_0 is the average number density of galaxies at the AGN redshift. Since the redshifts were not measured for galaxies, the projected cross-correlation function, ω , was derived from the observational data in the following way.

The projected cross-correlation function is obtained by integrating the equation (6) along the line of sight, then it is described as (Davis & Peebles 1983):

$$\omega(r_p) = 2 \int_0^{\infty} \xi(r_p, \pi) d\pi = 2 \int_{r_p}^{\infty} r dr \xi(r) (r^2 - r_p^2)^{-0.5}, \quad (7)$$

where r_p and π is components of distance from the AGN perpendicular to the line of sight and along the line of sight, respectively. We assumed a power law function for the density profile around an AGN, e.g. $\xi(r) = (r_0/r)^\gamma$.

In this case, equation (7) can be integrated analytically as:

$$\omega(r_p) = r_p \left(\frac{r_0}{r_p} \right)^\gamma \frac{\Gamma(1/2)\Gamma((\gamma-1)/2)}{\Gamma(\gamma/2)}, \quad (8)$$

where Γ is the Gamma function.

Studies of cross-correlation analysis published usually used a method which counted pairs of objects with a given separation ($DD(r)$) and compared with the expected background which is a number of pairs in a random sample for the same separation ($DR(r)$) (Davis & Peebles 1983),

$$\xi(r) = \frac{DD(r)}{DR(r)} - 1. \quad (9)$$

In this work, however, data of each AGN field are highly inhomogeneous, thus it is not appropriate to use the random catalog created from the whole dataset for estimating the background level. In addition, we need to consider two kinds of background. One is a background corresponding to $DR(r)$ in the equation (9), which is an average number density at the AGN redshift. We estimate this background ρ_0 as explained in section 3. The other background is an integrated number density of all the observed galaxies from $z = 0$ to infinity, which needs to be considered in our case as the redshifts of galaxies were not measured in our sample. The second background, n_{bg} , is estimated by fitting model function to the observed data. In addition, the coordinates of AGNs in our samples are well separated from each other, and the correlation function for each AGN can be calculated independently from the other AGN samples. Thus, in our case, it is enough to simply calculate the number density around each AGNs and take an average of them.

We measured number density of all the detected sources around AGNs of a given redshift range. The number density at perpendicular distance r_p from the i -th AGN is calculated as:

$$n_i(r_p) = N_i(r_p)/S_i(r_p), \quad (10)$$

where $N_i(r_p)$ is the number of detected sources at a distance range of $r_p \sim r_p + dr$ for the i -th AGN, $S_i(r_p)$ is the projected area corresponding to the distance range. Then the number density averaged over m AGNs of the same redshift range are given by:

$$n(r_p) = \frac{1}{m} \sum n_i(r_p) \quad (11)$$

The projected correlation function $\omega(r_p)$ averaged over the m AGNs was calculated as:

$$\omega(r_p) = \frac{n(r_p) - n_{bg}}{\sum \rho_{i,0}/m}, \quad (12)$$

$\rho_{i,0}$ is the averaged number density of observed galaxies at the i -th AGN redshift. $\rho_{i,0}$ was calculated for the rest frame wavelength corresponding to each observation band as described in section 3. The rest frame wavelength corresponding to the observation band was calculated by $\lambda_{rest} = \lambda_{center}/(1+z)$, where λ_{center} is the effective center wavelength of the observation band.

We used only the data observed at the most sensitive band for detecting the galaxies at the AGN redshift. The observation band with the largest value of $\rho_{i,0}$ was chosen as the most sensitive band. To show the depth of observations used in this work, m_{limit} of the observation with the most sensitive band is plotted against redshift in figure 10. Open circles represent AGNs for which UKIDSS survey data were used, and crosses represent AGNs for which Suprime-Cam data were used. The apparent magnitude corresponding to an absolute magnitude of -21 is shown as a dashed line. The number of AGN samples for each observation band are summarized in table 3.

In calculating $N_i(r_p)$, we took into account the coverage fraction for each annulus, $f_i(r_p)$, by multiplying $1/f_i(r_p)$ to a number of objects detected at a distance bin $r_p \sim r_p + dr$.

Galaxies near an AGN may be contaminated by the light of the AGN, and the detection efficiency for galaxies might be lowered there. Thus, in calculating $N_i(r_p)$, the region of 4 arcsec from the AGN was masked. The typical FWHM of the Suprime-Cam image used in this work is less than 1 arcsec, therefore the contamination effect of the AGN light to the galaxy detection efficiency would be negligible outside the masked region if the apparent brightness of the AGN is dimmer than 17 mag. The reduction of the projected area due to the masking was taken into account in the calculation of $S_i(r_p)$.

5. Results

We divided all the AGN samples into five redshift groups, $z = 0.3-0.6$ (referred to as z1), $0.6-0.9$ (z2), $0.9-1.3$ (z3), $1.3-1.8$ (z4) and $1.8-3.0$ (z5). For each redshift group, the dataset is further divided into a dimmer group ($M_V \geq -25$, referred by putting a suffix D after the redshift group name, e.g. z1-D) and a brighter group ($M_V < -25$, suffix B). In figure 5, the redshift and luminosity range of each group is shown with a solid box together with the absolute magnitude and redshift distribution of the AGNs. Hereafter we call an AGN of $M_V \geq -25$ as “dim AGN”, and an AGN of $M_V < -25$ “bright AGN”. The bright AGNs for $z < 0.6$ and the dim AGNs for $z \geq 1.3$ were not analyzed due to their poor statistics.

For each group the galaxy number density, $n(r_p)$, was calculated as a function of perpendicular comoving distance from the AGN, and it was fitted with a model function as described in the previous section. In the left panels of figures 11 and 12 the galaxy number density for each AGN group is shown with closed circles, and the model function fitted to the observation is shown with a solid line. The error bars represent one sigma statistical errors. The model function is derived from equations (8) and (12) as follows:

$$n(r_p) = r_p \left(\frac{r_0}{r_p} \right)^\gamma \frac{\Gamma(1/2)\Gamma((\gamma-1)/2)}{\Gamma(\gamma/2)} \bar{\rho}_0 + n_{bg}. \quad (13)$$

The horizontal dashed line in figures 11 and 12 represents the fitting parameter n_{bg} of equation (13). The bin size was fixed to 0.1 Mpc for redshift groups of z1 and z2, and

it was fixed to 0.2 Mpc starting from 0.1 Mpc for z3, z4 and z5 groups. For z3, z4 and z5 groups, the data of < 0.1 Mpc was ignored, since a large fraction of this distance range was masked to avoid the effect of AGN light.

In the right panels of the figures, the corresponding projected correlation functions $\omega(r_p)$ are also shown. We fixed the slope parameter γ to 1.8, which is a canonical value obtained from auto-correlation analysis among typical local galaxies by many other works (e.g. Zehavi et al. 2005). $\bar{\rho}_0$ is an average of $\rho_{i,0}$ for each AGN in the group, and it is fixed to the value calculated as described in section 3. The fitting parameters are summarized in table 4.

Evidence of galaxy clustering around the AGNs was detected with a 90% confidence level (C.L.) for all the groups except for z5-B. We obtained correlation lengths of $4.7^{+1.3}_{-0.7}$, $5.8^{+1.9}_{-1.1}$ and $7.6^{+3.2}_{-1.9}$ h⁻¹ Mpc for dim AGN groups of z1-D, z2-D, and z3-D, respectively. For bright AGN groups, correlation lengths of $6.3^{+2.4}_{-1.5}$, $5.1^{+2.7}_{-1.5}$, $11.1^{+6.1}_{-2.7}$ h⁻¹ Mpc were obtained for z2-B, z3-B, and z4-B, respectively. The errors quoted here indicate the sum of a systematic error estimated from uncertainty of ρ_0 and a statistical error of one sigma. For z5-B AGN group, no significant clustering signature was observed, and an upper limit of 13.1 h⁻¹ Mpc was obtained. This upper limits includes systematic error due to uncertainty of ρ_0 and statistical error of one sigma.

To examine the possibility that the clustering observed for z4-B was due to accidental alignment of high density regions, we analyzed eight independent offset fields of z4-B AGNs. The offset fields were taken apart from each AGN by 10 Mpc in the directions of right ascension and/or declination, so that the offset fields did not overlap with the high density region around AGN. We applied the same analysis procedure to these offset fields as was applied to the AGN fields. We derived density distributions averaged over each of the eight offset fields. The significance of excess or deficit at $r=0-2.5$ Mpc to the average density at $r=4-6$ Mpc were less than two sigmas, while the significance for the z4-B AGNs was 5.8σ . As no significant systematic excess was seen for the offset fields, we conclude that the excess seen for the AGN dataset is most likely due to galaxies associated with the AGNs.

We also examined the possibility that the excess was caused by only a single or a few samples which had large clustering. We calculated the average number density around z4-B AGNs for which absolute value of B_{QG} was less than or equal to 1000. The B_{QG} distribution for z4-B AGN samples is shown in figure 13, and 110 out of the 142 AGN samples satisfied this condition. The number density distribution is shown in figure 14. The excess at $r < 2.5$ Mpc is clearly found also for this relatively small clustering samples of $|B_{QG}| \leq 1000$. The calculated correlation length was $8.7^{+5.2}_{-2.5}$ h⁻¹ Mpc. From this result, we conclude that the excess seen in the z4-B sample is not created just from a single or a few samples with the largest clustering, but from a wide range of samples of z4-B group.

As described in section 2, 20% of the z4-B AGN samples are located in the Sextans field of RA = 150° – 157° and

Dec = -4° – +1°. To see the effect of the concentration to this specific field, we derived the distribution of number density for z4-B AGNs excluding the samples located in the Sextans field, and showed it in the left panel of figure 15. In the right panel of the same figure, the density distribution for z4-B AGNs located in the Sextans field is also shown. No significant difference is seen for the two density profiles. The cross correlation length for the z4-B samples excluding the AGNs of Sextans field is $10.0^{+2.6}_{-2.6}$ h⁻¹ Mpc, and it is consistent with the result for the whole z4-B samples. Thus, we can conclude that the result of z4-B is not strongly biased by the samples of the Sextans field.

In figure 16, the correlation length obtained for each AGN group is plotted as a function of redshift. The bright AGN samples (z2-B, z3-B, z4-B) are shown as closed circles, and the dim AGN samples (z1-D, z2-D, z3-D) are shown as closed triangles. The upper limit is shown for the z5-B sample. For comparisons, results of AGN-galaxy correlation analysis by other authors (Bornancini et al. 2007; Coil et al. 2007; Norman et al. 2009; Hickox et al. 2009) are also shown in the figure. The auto-correlation length of galaxy or QSO obtained by other authors (Ma et al. 2009; Zehavi et al. 2005; Hawkins et al. 2003; Wake et al. 2008; Ross et al. 2009; Shen et al. 2007) are also shown in the same figure.

It may not be appropriate to compare the clustering strength only with the correlation length, since it depends on the assumed or fitted slope parameter γ . The clustering strength is usually compared in σ_8 , which is the rms fluctuation of the galaxy distribution in the sphere with a comoving radius of $r_{max} = 8$ h⁻¹ Mpc, and calculated as (Miyaji et al. 2007; Peebles 1980).

$$\sigma_8^2 = (r_0/r_{max})^\gamma J_2 \quad (14)$$

$$J_2 = 72/[(3-\gamma)(4-\gamma)(6-\gamma)^2]. \quad (15)$$

Using these formulae, we converted a correlation length of each experiment to σ_8 , and they are compared in figure 17.

The results for low redshift samples ($z=0.3-0.9$, z1 and z2) are consistent with the existing measurements. Norman et al. (2009) measured the projected cross correlation between 420 QSOs and 4975 luminous red galaxies (LRG) at redshifts from 0.2 to 0.8 (an open square in figures 16 and 17) based on the data of 2QZ and 2SLAQ survey. Our measurements of σ_8 at $z=0.3-0.9$ (z1-D, z2-D, z3-B) agree with their value, although our galaxy sample is a mixture of dim galaxies detected with the Suprime-Cam and bright galaxies detected with the UKIDSS survey. Hickox et al. (2009) also measured the cross correlation of three types of AGNs and galaxies (asterisks in figures 16 and 17; from top to bottom radio, X-ray and IR selected AGNs) based on the AGN and Galaxy Evolution Survey (AGES) and Bootes multi-wavelength survey. Their sample contains 598 AGNs at redshift of 0.25 – 0.8. Our results are nearly consistent with their result.

The clustering of local galaxies measured by Ma et al. (2009) (K-band selected galaxy), Zehavi et al. (2005) (r-

band selected galaxy), and Hawkins et al. (2003) (b_J -band selected galaxy) are 5–7 Mpc (open diamonds in figure 16 from top to bottom, respectively). Our values for AGN-galaxy correlation length at $z = 0.3$ – 0.9 are, therefore, almost the same as the auto-correlation length of the local galaxies.

From the observational facts that at the local Universe red early-type galaxies are more clustered than blue late-type galaxies and bright galaxies are more clustered than dim galaxies, we can expect different clustering strength for UKIDSS and Suprime-Cam galaxies samples. To see the difference, we calculated the AGN-galaxy cross correlation function for UKIDSS selected galaxies and Suprime-Cam selected galaxies independently for z1-D and z2-D AGN groups. The results are summarized in table 3 and labeled as “OPT” for the Suprime-Cam galaxy samples and “IR” for the UKIDSS galaxy samples.

For the z1-D AGN group, larger correlation length was obtained for UKIDSS galaxies samples ($r_0 = 6.8^{+1.9}_{-1.0} \text{ h}^{-1}\text{Mpc}$) than that for Suprime-Cam galaxies samples ($r_0 = 3.0^{+1.5}_{-1.1} \text{ h}^{-1}\text{Mpc}$). The clustering of UKIDSS galaxies around z1-D AGNs is consistent with that of K-band selected galaxies measured by Ma et al. (2009) at the local Universe. As for the Suprime-Cam galaxies, the clustering is as small as that of dim galaxies ($M_r \geq -19$) measured by Zehavi et al. (2005). At this redshift range (z1), galaxies in the Suprime-Cam sample are dimmer than $M \sim -20$ as the brighter galaxies were masked before the source extraction, while the UKIDSS galaxy sample consists of bright galaxies ($M < -21$) (see top panel of figure 18). Thus the Suprime-Cam galaxies sample is strongly biased to dim galaxies (expected to be in the range of $M = -16 \sim -20$), while the UKIDSS sample is biased to bright galaxies ($M < -21$). The correlation length obtained for the Suprime-Cam galaxies can be consistent with the optically selected dim galaxies at the local Universe, if the luminosity dependence measured by Zehavi et al. (2005) is taken into account.

As for the z2-D group, correlation length of $7.4^{+4.7}_{-2.1}$ and $5.0^{+1.6}_{-1.0} \text{ h}^{-1}\text{Mpc}$ were obtained for the UKIDSS and Suprime-Cam samples, respectively. The difference was smaller than that of the z1-D group, and they were nearly consistent within their uncertainties. At this redshift range, maximum brightness of the Suprime-Cam galaxies comes down to $M \sim -22$, which almost equals or is brighter than the characteristic luminosity L_* (break point of luminosity function). Thus, it is expected that the clustering of Suprime-Cam galaxies is enhanced due to the increase in the fraction of bright galaxies in the sample. We conclude that the difference between the clustering properties of UKIDSS and Suprime-Cam galaxies can be explained by the luminosity dependence of galaxy clustering as observed in the local Universe.

The result for z3-D is significantly larger than the result by Coil et al. (2007). They measured quasar-galaxy cross correlation length from 52 QSOs at redshifts from 0.7 to 1.4 based on the SDSS and DEEP2 survey (an open triangle in figures 16 and 17). The range of absolute magnitude

of AGNs used in Coil et al. (2007) is from -26 to -20 , which is almost equivalent to our dim AGN sample. Coil et al. (2007) measured the correlation length using the data at a distance scale from 0.1 to 10 Mpc. They used γ as a free parameter, then obtained 1.55 for γ . Thus we fit the model function to our data of 0.1 to 3.5 Mpc with a fixed γ of 1.55. Then we obtained much longer correlation length, which is not consistent with the result by Coil et al. (2007). The difference may come from the difference of galaxy samples used. The DEEP2 galaxies sample is selected by adapting a color cut, and it is expected that redder galaxies are more dominant in their sample than in ours.

It should be noted that our clustering measurement is dominated by dim galaxies near the detection threshold, while the other experiment conducting spectroscopic observations is mostly targeted to the bright end of the luminosity function. Therefore, our measurement has sensitivity to the clustering properties of relatively dim galaxies which are not measured by spectroscopic observations. In addition to that, our optical measurement is biased to blue galaxy at this redshift range, thus it is expected that star-forming galaxies are dominant in our galaxy sample.

In the case of spectroscopic observation, a red galaxy is preferentially selected as a target since the redshift estimate for a red galaxy is more robust than that for a blue galaxy owing to the existence of a sharp 4,000 Å break in the spectrum.

The difference between our measurement and that of Coil et al. (2007) may be attributed to the difference in the clustering properties of a dimmer-blue galaxy and a bright-red galaxy. It is also possible that the difference is due to the cosmic variance, as the number of well separated fields is only four for the DEEP2 dataset.

The $\sigma_{8,\text{AGN-G}}$ obtained for the z3-D is almost comparable with $\sigma_{8,\text{Q}}$ derived from the QSO auto-correlation length by Ross et al. (2009), and with $\sigma_{8,\text{G}}$ derived from the auto-correlation length of radio-quiet Luminous Red Galaxies (LRG) at lower redshift by Wake et al. (2008). The correlation length for the bright AGN group at the same redshift (z3-B) was consistent with that for z3-D group, and no significant evidence of AGN luminosity dependence was found. Shen et al. (2009) examined luminosity dependence of the clustering of SDSS QSOs. They also found no significant evidence for the luminosity dependence, which is consistent with our observation.

The distribution of galaxy number density for the bright AGN group at redshift 1.3–1.8 (z4-B) shows relatively flat excess at < 2.5 Mpc. This feature may indicate that a significant number of the AGNs are not located at the center of a galaxy group but distributed over a scale of 5 Mpc.

Bornancini et al. (2007) have examined the correlation between the 13 SDSS QSOs and the distant red galaxies (DRG; $J - K_s > 2.3$) at redshifts from 1 to 2 (an open circle in figures 16 and 17). Their AGN sample has a luminosity range similar to our bright AGN sample. They reported a correlation length of $5.4 \pm 1.6 \text{ h}^{-1}\text{Mpc}$. Considering that the redshift range of their sample extends over z3 and

z4 of our samples, we calculated a correlation length and $\sigma_{8, \text{AGN-G}}$ for a combined sample of z3-B and z4-B to be $7.5^{+3.3}_{-1.6} \text{h}^{-1} \text{Mpc}$ and $1.3^{+0.5}_{-0.3}$, respectively. Although this result is almost consistent with the value of Bornancini et al. (2007) within the quoted error, the distribution of number density shows a flat excess at 1–2.5 Mpc (figure 19), which was significant for z4-B sample and barely seen also in the z3-B sample. This feature was not observed in the data of Bornancini et al. (2007). The magnitude range of galaxy sample used by Bornancini et al. (2007) is $K \leq 19.5(\text{Vega}) \sim 21.4(\text{AB})$, while our galaxy sample of Suprime-Cam is dimmer than $m_{\text{AB}} \sim 22$ on average. Thus the difference in the number density profile might be due to the difference in brightness and/or observation band of the galaxy samples.

The clustering strength, $\sigma_{8, \text{AGN-G}}$, obtained for z4-B sample is nearly consistent within the quoted error with the QSO clustering $\sigma_{8, \text{Q}}$ calculated from the observational result by Ross et al. 2009 at the same redshift.

For the AGN group at redshift 1.8–3.0 (z5-B), we could not find any evidence of a clustering signature. At this high redshift range, the number of galaxies which are brighter than the limiting magnitude is very poor, and the clustering signal easily disappears due to the foreground galaxies.

The detection limit of galaxies for a lower redshift group is dimmer in absolute magnitude than that for a higher redshift group. From observations of the local Universe, it is known that brighter galaxies usually have stronger clustering. Zehavi et al. 2005 analyzed data from SDSS DR2 and derived the luminosity dependence of the galaxy clustering. They showed that the galaxy-galaxy correlation function increases continuously with luminosity, and above the characteristic luminosity L_* ($M_r \sim -20.5$) it increases more rapidly. The measured correlation lengths were $9.81 \pm 0.39 \text{h}^{-1} \text{Mpc}$ for $M_r < -22$, decreased rapidly down to 6.16 ± 0.17 for $-22 < M_r < -21$, and decreased rather slowly down to 2.68 ± 0.39 for $-18 < M_r < -17$. Thus it is expected that the clustering of galaxies around AGNs can be stronger at higher redshift due to the galaxy selection effect.

In figure 20, the distributions of averaged number density of bright ($m < -21 + DM$, left panel) and dim ($m \geq -21 + DM$, right panel) galaxies around the AGNs are shown for z4-B AGN group. The range of absolute magnitude for both samples can be inferred from the bottom panel of figure 18, which shows the distribution of $m - DM(z)$ for R-band observations. They are expected to be in the range of $-24 - -21$ and $-21 - -19$ for the bright and dim galaxy samples, respectively. As can be seen from this figure, the excess number densities observed for dim and bright galaxy samples is almost comparable. The excess of source count at $r_p < 2.5 \text{Mpc}$ is 9.3 ± 1.2 and 7.0 ± 1.2 for the dim and bright galaxy sample, respectively. Thus half of the clustering found for the z4-B sample is contributed from bright galaxies with absolute magnitude less than -21 .

It should be noted that this does not necessarily mean that the clustering strength of dim galaxy sample and

bright galaxy sample is equivalent, because the average numbers of detectable galaxies at the AGN redshift are different for the two samples. Since ρ_0 for each of the bright and dim galaxy sample cannot be determined by the method as shown in section 3, we estimated the upper limit for the number density of bright galaxies ($M < -21$) by choosing smaller one of the followings: integral of the luminosity function up to $M = -21$ or ρ_0 calculated for the whole galaxies as described in section 3. Then we obtained the upper limit of the average number density for the bright galaxies of z4-B sample as $\sim 0.26 \times 10^{-3} \text{Mpc}^{-2}$. The average density estimated for the whole galaxies sample is $1.3 \times 10^{-3} \text{Mpc}^{-2}$, thus the number density of the bright galaxies is less than 1/4 of the dim galaxies ($M \geq -21$).

The lower limit of correlation length for the bright galaxy sample was calculated as $18 \text{h}^{-1} \text{Mpc}$ by adapting $\rho_0 = 0.26 \times 10^{-3} \text{Mpc}^{-2}$ in the model fitting. This correlation length is significantly larger than that measured for a bright galaxy at the local Universe. Therefore the degree of increase in correlation length for z4-B relative to those for the low redshift samples is larger than that expected from the galaxy luminosity dependence observed in the local Universe.

There would be another possibility that the redshift dependence is caused by selection bias to a type of galaxy, that is, early or late type galaxy. It is known that the early type galaxies are clustered stronger than the late type galaxies at the local Universe. Although we used UKIDSS IR data, the observations were too shallow to detect the high redshift galaxies and they were almost not used for the high redshift samples. Thus our high redshift dataset is biased to blue-colored late type galaxies. This is contrary to the expectation that the larger correlation length for z4-B group is due to the selection bias to the redder galaxies which are strongly clustered in the local Universe.

6. Discussion

We showed that the low redshift AGNs ($z = 0.3\text{--}0.9$, z1 and z2) had clustering properties similar to that of a typical local galaxy. This would imply that these AGNs are located in dark matter halos which have a mass similar to that occupied by typical galaxies at the local Universe, provided that there is a correlation between the clustering property and the mass of the dark matter halo as suggested by many numerical simulations.

No significant AGN luminosity dependence was observed for z2 and z3 redshift samples. Since the luminosity of AGN is not constant and evolving with time, it may be possible for AGNs with different luminosities to have similar environments and to be powered by the same mechanism at some epoch of their evolution. The QSO lifetime, t_{Q} , which is a timescale for the most luminous phase of the activity, is expected to be in the range from $10^6 - 10^8$ yr (Martini 2004). For a duration much longer than the period of the most luminous phase, AGNs are obscured by surrounding gas and dust, and thus they are observed

as low luminosity AGNs or other types of galaxies such as sub-mm galaxies, or they cannot be observed completely. Therefore, no detection of the luminosity dependence of the clustering supports the theoretical expectation of the short QSO lifetime.

We also showed that the bright AGNs at redshift 1.3–1.8 (z4-B) have relatively denser environments than typical local galaxies, and that the clustering strength was much larger for bright galaxies ($M < -21$) than dim galaxies ($M \geq -21$). The lower limit of the cross correlation length of AGN and the bright galaxies was $18 \text{ h}^{-1}\text{Mpc}$, which is extremely large compared to the local bright galaxies measured by Zehavi et al. (2005). Considering that our dataset is biased to blue star-forming galaxies at higher redshift, we deduce that the clustering of blue star-forming galaxies is enhanced around the high redshift AGNs.

Under these circumstances, the chance of a major merger is expected to be enhanced relative to that at low redshift, thus the major merger could be a preferred mechanism to trigger the AGN activity at this redshift range. This result indicate that there exists redshift dependence for the environment of AGNs, that is, at higher redshift ($z > \sim 1.3$) larger fraction of AGNs are produced in a more crowded region with blue star-forming galaxies, while at lower redshift they are mostly produced in an environment which is common at the local Universe. AGNs at low redshift might be powered by different mechanism from high redshift AGNs, e.g. a secular process such as bars or other disk instabilities.

The $\omega(r_p)$ profiles of z4-B show deviations from a power law function, which shows a flat over density at $r_p < 2.5 \text{ Mpc}$. This property could be attributed to the distribution of AGN location in a dark matter halo; there may be a considerable number of AGNs which have an offset of $\sim 2.5 \text{ Mpc}$ from the center of galaxy distribution or a dark matter halo.

The $\omega(r_p)$ for bright AGN samples have a tendency to show a deficit of galaxy at the smallest distance bin. This feature is not seen for any of the dim AGN samples. This also might be explained by distribution of AGN location inside the dark matter halo. Galaxy formation near the bright AGN may also be suppressed due to the strong radiation from the AGN.

In this work, the error of r_0 is large compared to the experiments measuring the redshift of all the target galaxies. This is mostly due to the uncertainty of determination ρ_0 , thus the accuracy of ρ_0 needs to be improve. For that purpose, we need to calibrate the ρ_0 estimated as described in section 3 experimentally. Once the ρ_0 estimation is calibrated and the accuracy is evaluated for each AGN field, it would be possible to reduce the uncertainty of ρ_0 by a factor two.

7. Conclusions

Using the Japanese Virtual Observatory, we were able to measure the clustering property for $\sim 1,809$ AGNs at redshifts 0.3–3.0 with optical brightness of $M_V = -30$ to -20 . The AGN samples were divided into five redshift

groups (z1–z5), and each redshift group was further divided into two brightness groups (e.g. z1-D, z2-D, z2-B ...).

We found evidence of clustering except for the highest redshift group (z5-B). The correlation lengths between the AGNs and galaxies were measured for each group. We found that the clustering strength of the high redshift samples (z4-B) was larger than that of the low redshift sample (z1-D), and it was nearly consistent with that of QSO clustering at the same redshift. We also showed that bright galaxies of absolute magnitude ($M_{AB} < -21$) were more densely clustered than the dimmer galaxies for the case of z4-B AGN group. Considering that, at higher redshift ($z > 1$), the data used in this work are based on optical observations and blue galaxies are expected to be preferentially detected in our dataset, we can deduce that blue star-forming galaxies are highly clustered around the AGNs at these redshifts. This clustering feature is different from that seen for the low redshift AGNs.

The deviation of $\omega(r_p)$ from the power law function was seen in the result of z4-B samples, and there was an indication for suppression of cross-correlation at the smallest distance bin for the bright AGN samples. These features could be related to the distribution of AGN location in a dark matter halo, and could be related to fueling mechanism of the AGN. If a significant fraction of AGNs was located offset from the center of a dark matter halo or a galaxy distribution, the deviation from power law could be seen. It is also possible that the galaxy formation near the AGN was suppressed due to the strong radiation of the AGN.

We showed that the analysis method presented in this paper can be a powerful probe for the small scale environment of the high redshift AGNs. Our method can be used for tracing dim and blue star-forming galaxies at small scale ($r < 1 \text{ Mpc}$), while the spectroscopic observations provide a precise information about large scale clustering properties for bright and red early type galaxies. These two types of observations, therefore, are complementary, and can provide important clues to understanding the origin of the AGN activity.

To derive more definite evidence for the AGN-galaxy clustering with this method, more observational data are needed in view of the quantity and quality. Highly homogeneous observations of a huge number of AGN fields will be conducted with the Hyper Suprime-Cam, which will be installed on the Subaru Telescope around 2011. This survey project will give more definite observational evidence on the evolution of an AGN.

Acknowledgments

This work was supported by the JSPS Core-to-Core Program and Grant-in-aid for Information Science (15017289, 16016292, 18049074 and 19024070) carried out by the Ministry of Education, Culture, Sports, Science and Technology (MEXT) of Japan. YS is grateful for support under Grant-in-aid for Young Scientists (B) (17700085, 21740143) carried out by the MEXT of Japan.

References

- Abazajian, K., et al., 2004, *AJ*, 128, 502
- Abazajian, K. N., et al., 2009, *ApJS*, 182, 543
- Adelberger, K. L., & Steidel, C. C., 2005, *ApJ*, 630, 50
- Arp, H. C., Burbidge, E. M., Chu, Y., Zhu, X., 2001, *ApJ*, 553, 11
- Bade, N., Fink, H. H., Engels, D., Voges, W., Hagen, H.-J., Wisotzki, L., Reimers, D., 1995, *A&AS*, 110, 469
- Barger, A. J., Cowie, L. L., Brandt, W. N., Capak, P., Garmire, G. P., Hornschemeier, A. E., Steffen, A. T., Wehner, E. H., 2002, *AJ*, 124, 1839
- Barnes, J. E., Hernquist, L. E., 1991, *ApJ*, 370, 65
- Barnes, J. E. & Hernquist, L. E., 1996, *ApJ*, 471, 115
- Barr, J. M., Bremer, M. N., Baker, J. C. & Lehnert, M. D., 2003, *MNRAS*, 346, 229
- Barton, E. J., van Zee, L., Bershad, M. A., 2006 *ApJ*, 649, 129
- Bauer, F. E., Condon, J. J., Thuan, T. X., Broderick, J. J., 2000, *ApJS*, 129, 547
- Becker, R. H., et al., 2001, *ApJS*, 135, 227
- Bertin, E. & Arnouts, S., 1996, *A&AS*, 117, 393
- Best, P. N., Kauffmann, G., Heckman, T. M., Brinchmann, J., Charlot, S., Ivezić, Z., White, S. D. M., 2005, *MNRAS*, 362, 25
- Bolzonella, M., Miralles, J.-M. & Pello, R., 2000, *A&A*, 363, 476
- Bornancini, C. G. & Lambas, D. G., 2007, *MNRAS*, 377, 179
- Bower, R. G., et al., 1996, *MNRAS*, 281, 59
- Boyle, B. J., Fong, R., Shanks, T., Peterson, B. A., 1990, *MNRAS*, 243, 1
- Branduardi-Raymont, G., Mason, K. O., Murdin, P. G., Martin, C., 1985, *MNRAS*, 216, 1043
- Brown, M. J. I., Webster, R. L., Boyle, B. J., 2000, *MNRAS*, 317, 782
- Brown, M. J. I., Boyle, B. J., Webster, R. L., 2001, *AJ*, 122, 26
- Buchalter, A., Helfand, D. J., Becker, R. H., White, R. L., 1998, *ApJ*, 494, 503
- Budavari, T., et al., 2003, *ApJ*, 595, 59
- Caccianiga, A., et al., 2004, *A&A*, 416, 901
- Cirasuolo, M. et al., 2007, *MNRAS*, 380, 585
- Coil, A. L. et al., 2007, *ApJ*, 654, 115
- Coil, A. L., et al., 2009, *ApJ*, 701, 1484
- Coldwell, G. V. & Lambas, D. G., 2006, *MNRAS*, 371, 786
- Collinge, M. J., et al., 2005, *AJ*, 129, 2542
- Cowie, L. L., Songaila, A., Hu, E. M., & Cohen, J. G., 1996 *AJ*, 112, 839
- Crampton, D., Gussie, G.; Cowley, A. P.; Schmidtke, P. C., 1997, *AJ*, 114, 2353
- Crawford, C. S., Gandhi, P., Fabian, A. C., Wilman, R. J., Johnstone, R. M., Barger, A. J., Cowie, L. L., 2002, *MNRAS*, 333, 809
- Cristiani, S., Barbieri, C., La Franca, F., Iovino, A., Nota, A. et al., 1989, *A&AS*, 77, 161
- Cristiani, S., et al., 1995, *A&AS*, 112, 347
- Croom, S. M. et al., 2004, *MNRAS*, 349, 1397
- Croom, S. M. et al., 2005, *MNRAS*, 356, 415
- Croton, D. J., et al., 2006, *MNRAS*, 365, 11
- Davis, M. & Peebles, P. J. E., 1983, *ApJ*, 267, 465
- Dewangan, G. C., Singh, K. P., Jones, L. R., McHardy, I. M., Mason, K. O., Newsam, A. M., 2001, *MNRAS*, 325, 1616
- Dressler, A., Gunn, J. E., 1992, *ApJS*, 78, 1
- Eckart, M. E., Stern, D., Helfand, D. J., Harrison, F. A., Mao, P. H., Yost, S. A., 2006, *ApJS*, 165, 19
- Ellingson, E., Yee, H. K. C., Green, R. F., 1991, *ApJ*, 371, 49
- Enoki, M., Nagashima, M., & Gouda, N., 2003, *PASJ*, 55, 133
- Fiore, F., et al., 2003, *A&A*, 409, 79
- Fisher, K. B., Bahcall, J. N., Kirhakos, S., Schneider, D. P., 1996, *ApJ*, 468, 469
- Gabasch, A. et al., 2004, *A&A*, 421, 41
- Gabasch, A. et al., 2006, *A&A*, 448, 101
- Georgantopoulos, I., Georgakakis, A., Akylas, A., Stewart, G. C., Giannakis, O., Shanks, T., Kitsionas, S., 2004, *MNRAS*, 352, 91
- Gilli, R., et al., 2005, *A&A*, 430, 811
- Gilli, R., et al., 2009, *A&A*, 494, 33
- Gioia, I. M., Henry, J. P., Mullis, C. R., Bohringer, H., Briel, U. G., Voges, W., Huchra, J. P., 2003, *ApJS*, 149, 29
- Glikman, E., Gregg, M. D., Lacy, M., Helfand, D. J., Becker, R. H., White, R. L., 2004, *ApJ*, 607, 60
- Granato, G. L., De Zotti, G., Silva, L., Bressan, A., Danese, L., 2004, *ApJ*, 600, 580
- Grazian, A., Negrello, M., Moscardini, L., Cristiani, S., Haehnelt, M. G., Matarrese, S., Omizzolo, A., Vanzella, E., 2004, *AJ*, 127, 592
- Grindlay, J. E., 1993, *A&AS*, 97, 113
- Hall, P. B., et al., 1996 *ApJ*, 462, 614
- Hall, P. B., et al., 2000, *AJ*, 120, 2220
- Hasinger, G., Bergeron, J., Mainieri, V., Rosati, P., Szokoly, G., Cdfs Team, 2002, *The Messenger*, No.108, p.11
- Hawkins, E., et al., 2003, *MNRAS*, 346, 78
- He, X.-T., Cannon, R. D., Peacock, J. A., Smith, M. G., Oke, J. B., 1984, *MNRAS*, 211, 443
- Healey, S. E., et al., 2008, *ApJS*, 175, 97
- Hennawi, J. F. et al., 2006 *AJ*, 131, 1
- Hes, R., Barthel, P. D., Fosbury, R. A. E., 1996, *aap*, 313, 423
- Hewett, P. C., et al., 1991, *AJ*, 101, 1121
- Hewett, P. C., Foltz, C. B., Chaffee, F. H., 1995, *AJ*, 109, 1498
- Hickox, R. C. et al., 2009, *ApJ*, 696, 891
- Hoag, A. A., Thomas, N. G., Vaucher, B. G., 1982, *ApJ*, 263, 23
- Hopkins, P. F., Hernquist, L., Cox, T. J., and Keres, D., 2008, *ApJS*, 175, 356
- Hornschemeier, A. E., et al., 2001, *ApJ*, 554, 742
- Hutchings, J. B., Crampton, David, Morris, S. L., Durand, D., Steinbring, E., 1999 *AJ*, 117, 1109
- Kashikawa, N. et al., 2004 *PASJ*, 56, 1011
- Kashikawa, N. et al., 2006, *ApJ*, 637, 631
- Kauffmann, G., Heckman, T. M., Best, P. N., 2008, *MNRAS*, 384, 953
- Kauffmann, G., and Haehnelt, M. G., 2000, *MNRAS*, 311, 576
- Kauffmann, G., & Haehnelt, M. G., 2002, *MNRAS*, 332, 529
- Kniazev, A. Y., et al., 2004, *ApJS*, 153, 429
- Kodama, T. et al., 2004, *MNRAS*, 350, 1005
- Kormendy & Richstone, 1995, *ARA&A* 33, 581
- Krumpe, M., Miyaji, T., Coil, A. L., 2010, *ApJ*, 713, 558
- La Franca, F., Cristiani, S., Barbieri, C., 1992, *AJ*, 103, 1062
- La Franca, F., et al., 2002, *ApJ*, 570, 100
- Lehmann, I., Hasinger, G., Schmidt, M., Gunn, J. E., Schneider, D. P., Giacconi, R., McCaughrean, M., Trmper, J., Zamorani, G., 2000, *A&A*, 354, 35
- Lehmann, I., et al., 2001, *A&A*, 371, 833
- Leipski, C., et al., 2005, *A&A*, 440, 5
- Liu, C. T., Petry, C. E., Impey, C. D., Foltz, C. B., 1999, *AJ*, 118, 1912

- Lynden-Bell D., 1969, *Nature*, 223, 690
- Lynds, C. R., Hill, S. J., Heere, K., Stockton, A. N., 1966, *ApJ*, 144, 1244
- Ma, B. et al., 2009, *Research in Astronomy and Astrophysics*, 9, 979
- Madgwick, D. S., et al., 2003, *MNRAS*, 344, 847
- Martini, P. 2004, in *Coevolution of Black Holes and Galaxies*, ed. L. C. Ho (Cambridge: Cambridge Univ. Press), 170
- Marziani, P., Sulentic, J. W., Dultzin-Hacyan, D., Calvani, M., Moles, M., 1996, *ApJS*, 104, 37
- Mason, K. O., et al., 2000, *MNRAS*, 311, 456
- McHardy, I. M., et al., 1998, *MNRAS*, 295, 641
- McIntosh, D. H., Impey, C. D., Petry, C. E., 2004, *AJ*, 128, 544
- McLure, R. J. & Dunlop, J. S., 2001, *MNRAS*, 321, 515
- Miller, E. D., Bregman, J. N., Knezek, P. M., 2002, *ApJ*, 569, 134
- Miller, C. J. et al., 2003, *ApJ*, 597, 142
- Miyaji, T., et al., 2007, *ApJS*, 172, 396
- Molthagen, K., Wendker, H. J., Briel, U. G., 1997, *A&AS*, 126, 509
- Monk, A. S., Penston, M. V., Pettini, M., Blades, J. C., 1988, *MNRAS*, 234, 193
- Mullis, C. R., Henry, J. P., Gioia, I. M., Bohringer, H., Briel, U. G., Voges, W., Huchra, J. P., 2004, *ApJ*, 617, 192
- Myers, A. D., Brunner, R. J., Richards, G. T., Nichol, R. C., Schneider, D. P., Vanden Berk, D. E., Scranton, R., Gray, A. G., Brinkmann, J., 2006 *ApJ*, 638, 622
- Myers, A. D., Brunner, R. J., Nichol, R. C., Richards, G. T., Schneider, D. P., Bahcall, N. A., 2007, *ApJ*, 658, 85
- Norberg, P., et al., 2002, *MNRAS*, 332, 827
- Norman, D. J., Proprius, R. De, & Ross, N. P., 2009, *ApJ*, 695, 1327
- Ouchi, M. et al., 2004, *ApJ*, 611, 660
- Overzier, R. A., Rottgering, H. J. A., Rengelink, R. B., Wilman, R. J., 2003, *A&A*, 405, 530
- Padmanabhan, N., White, M., Norberg, P., & Porciani, C., 2009, *MNRAS*, 397, 1862
- Peebles, P. J. E., 1980, *The large-scale structure of the universe* (Princeton: Princeton University Press,)
- Prescott, M. K. M., et al., 2006 *ApJ*, 644, 100
- Rees, M.J., 1984, *ARA&A*, 22, 471
- Reyes, R., et al., 2008, *AJ*, 136, 2373
- Richards, G. T., et al., 2001, *AJ*, 121, 2308
- Richards, G. T. et al., 2006, *AJ*, 131, 2766
- Richstone et al., 1998, *Nature*, 395, 14
- Ross, N. P. et al., 2009, *ApJ*, 697, 1634
- Rowan-Robinson, M., et al.2004, *MNRAS*, 351, 1290
- Rowan-Robinson, M., 2004, *MNRAS*, 351, 1290
- Salpeter, E. E., 1964, *ApJ*, 140, 796
- Sanders, D. B., Soifer, B. T., Elias, J. H., Madore, B. F., Matthews, K., Neugebauer, G., Scoville, N. Z., 1988, *ApJ*, 325, 74
- Schmidt, M., Schneider, D. P., Gunn, J. E., 1986, *ApJ*, 206, 411
- Schmidt, M., et al.1998, *A&A*, 329, 495
- Schneider, D. P., Schmidt, M., Gunn, J. E., 1994, *AJ*, 107, 1245
- Schneider, D. P., et al., 2005, *AJ*, 130, 367
- Schneider, D. P. et al., 2007 *AJ*, 134, 102
- Serber, W., Bahcall, N., Menard, B., and Richards, G., 2006, *ApJ*, 643, 68
- Sharp, R. G., et al., 2002, *MNRAS*, 337, 1153
- Shen, Y. et al., 2007, *ApJ*, 133, 2222
- Shen, Y. et al., 2009, *ApJ*, 697, 1656
- Shirasaki, Y. et al., 2008, *Fusion Engineering and Design*, 83, 438
- Silverman, J. D. et al., 2005, *ApJ*, 618, 123
- Sorrentino, G., Radovich M., & Rifatto A., 2006, *A&A*, 451, 809
- Springel, V., Di Matteo, T., Hernquist, L., 2005, *ApJL*, 620, L79
- Steffen, A. T., Barger, A. J., Capak, P., Cowie, L. L., Mushotzky, R. F., Yang, Y. *AJ*, 128, 1483
- Strand, N. E., Brunner, R. J. & Myers, A. D., 2008, *ApJ*, 688, 180
- Ueda, Y. et al., 2003, *ApJ*, 598, 886
- Usher, P. D., Green, R. F., Huang, K. L., Warnock, A., III, 1983, *Quasars and gravitational lenses; Proceedings of the Twenty-fourth Liege International Astrophysical Colloquium, Cointe-Ougree, Belgium, June 21-24, 1983 (A85-13301 03-90). Cointe-Ougree, Belgium, Universite de Liege*, 245
- Veron, P., et al., 1990, *A&AS*, 86, 543
- Veron-Cetty, M.-P. and Veron, P. *A&A*, 455, 773
- Wake, D. A., et al., 2008, *MNRAS*, 391, 1674
- Warren, S. J. et al., 2007, *arXiv:astro-ph/0703037*
- Watanabe, S., Akiyama, M., Ueda, Y., Ohta, K., Mushotzky, R., Takahashi, T., Yamada, T., 2002, *PASJ*, 54, 683
- White, R. L., et al., 2000, *ApJS*, 126, 133
- Williams, R.J., Pogge, R. W., Mathur, S., 2002, *AJ*, 124, 3042
- Wold, M., Lacy, M., Lilje, P. B., Serjeant, S., 2000, *MNRAS*, 316, 267
- Wold, M., Lacy, M., Lilje, P. B., Serjeant, S., 2001, *MNRAS*, 323, 231
- Yagi, M. et al., 2002, *AJ*, 123, 66
- Yang, Y., Mushotzky, R. F., Barger, A. J., Cowie, L. L., 2006, *ApJ*, 645, 68
- Yee, H. K. C., Green, R. F., 1984, *ApJ*, 280, 79
- Yee, H. K. C., Green, R. F., 1987, *ApJ*, 319, 28
- Zakamska, N. L., et al., 2003, *AJ*, 126, 2125
- Zehavi, I., et al., 2002, *ApJ*, 571, 172
- Zehavi, I., et al., 2005, *ApJ*, 630, 1
- Zhan, Y.; Chen, J.-S., 1987, *Chinese Astronomy and Astrophysics*, 11, 299
- Zhan, Y., Chen, J.-S., 1989, *Chinese Astronomy and Astrophysics*, 13, 139
- Zhou, H., Wang, T., Yuan, W., Lu, H., Dong, X., Wang, J., Lu, Y., 2006, *ApJS*, 166, 128

Table 1. Distance ranges for background estimation in the calculation of B_{QG}

redshift group	redshift range	$r_{bg,min}$ Mpc	$r_{bg,max}$ Mpc
z1	0.3 – 0.6	1.5	2.5
z2	0.6 – 0.9	2.0	3.5
z3	0.9 – 1.3	3.0	5.0
z4	1.3 – 1.8	4.0	6.0
z5	1.8 – 3.0	4.0	6.0

Table 2. Number of AGNs selected from SDSS, 2dF, other optical, X-ray and radio observations for each redshift and AGN luminosity group.

group	SDSS *	2dF †	UV-OPT-IR ‡	XRAY §	RADIO	Total
z1-D	478 (73.5%)	51 (7.8%)	96 (14.7%)	20 (3.1%)	6 (0.9%)	651
z2-D	334 (79.5%)	66 (15.7%)	13 (3.1%)	7 (1.7%)	0 (0.0%)	420
z3-D	68 (68.0%)	20 (20.0%)	9 (9.0%)	3 (3.0%)	0 (0.0%)	100
z2-B	101 (89.4%)	4 (3.5%)	2 (1.8%)	2 (1.8%)	4 (3.5%)	113
z3-B	234 (85.4%)	32 (11.7%)	4 (1.5%)	2 (0.7%)	2 (0.7%)	274
z4-B	107 (75.4%)	21 (14.8%)	10 (7.0%)	4 (2.8%)	0 (0.0%)	142
z5-B	76 (69.7%)	21 (19.3%)	8 (7.3%)	4 (3.7%)	0 (0.0%)	109
total	1398 (77.3%)	215 (11.9%)	142 (7.8%)	42 (2.3%)	12 (0.7%)	1809

* Number of AGN samples contained in the SDSS DR5 QSO catalog (4th Ed.) (Schneider et al. 2007). This number includes samples contained also in the 2dF QSO catalog.

† Number of AGN samples contained in the 2dF QSO catalog (Croom et al. 2004) and not contained in the SDSS QSO catalog.

‡ Number of AGN samples selected based on the optical properties. References of each AGN are: Zakamska et al. 2003, Reyes et al. 2008, Abazajian et al. 2004, Collinge et al. 2005, Schneider et al. 2005, Prescott et al. 2006, Barton et al. 2006, Zhan and Chen 1989, Williams et al. 2002, Richards et al. 2001, Hall et al. 2000, Veron et al. 1990, Rowan-Robinson et al. 1990, McIntosh et al. 2004, Liu et al. 1999, Leipski et al. 2005, La Franca et al. 1992, Kniazev et al. 2004, Hewett et al. 1995, Cristiani et al. 1995, Boyle et al. 1990, Hennawi et al. 2006, Hall et al. 1996, Zhan et al. 1987, Schneider et al. 1994, Hewett et al. 1991, Sharp et al. 2002, Abazajian et al. 2009, Hoag et al. 1982, Usher et al. 1983, Monk et al. 1988, He et al. 1984, Dressler & Gunn 1992, Cristiani et al. 1989 Zhou et al. 2006 Schmidt et al. 1986

§ Number of AGN samples selected based on X-ray observations. References of each AGN are: Silverman et al. 2005, Steffen et al. 2004, Lehmann et al. 2000, Watanabe et al. 2002, Schmidt et al. 1998, Molthagen et al. 1997, Lehmann et al. 2001, La Franca et al. 2002, Hasinger et al. 2002, Grindlay 1993, Gioia et al. 2003, Eckart et al. 2006, Dewangan et al. 2001, Crawford et al. 2002, Caccianiga et al. 2004, Branduardi-Raymont et al. 1985, Bauer et al. 2000, Barger et al. 2002, McHardy et al. 1998, Miller et al. 2002, Georgantopoulos et al. 2004, Fiore et al. 2003, Bower et al. 1996, Bade et al. 1995, Mason et al. 2000, Arp et al. 2001, Crampton et al. 1997,

|| Number of AGN samples selected from Radio observations. References of each AGN are: Becker et al. 2001, Glikman et al. 2004, Healey et al. 2008, Hes et al. 1996, Lynds et al. 1966, Marziani et al. 1996, Rowan-Robinson et al. 2004, White et al. 2000, Wold et al. 2000 Buchalter et al. 1998

Table 3. Number of AGN samples for each AGN group and observation band.

group	B	V	R	I	i'	z'	K
z1-D	13	7	21	9	13	4	584
z2-D	0	6	18	16	4	2	374
z3-D	2	3	4	6	5	4	76
z2-B	1	1	9	7	3	1	91
z3-B	10	15	25	19	11	8	186
z4-B	11	15	45	32	21	9	9
z5-B	12	19	38	18	12	5	5

Table 4. Fitting parameters of projected cross correlation analysis

group	z	\bar{z}^*	M_V^\dagger	n_{AGN}^\ddagger mag	r_0^\parallel $h^{-1}\text{Mpc}$	n_{bg}^\S Mpc^{-2}	$\bar{\rho}_0^\#$ Mpc^{-3}
z1-D	0.3 – 0.6	0.46	–25.0 – –20.0	651	$4.7^{+1.3}_{-0.7}$	22.1 ± 0.07	$4.3^{+0.7}_{-1.1}$
z2-D	0.6 – 0.9	0.73	–25.0 – –20.0	420	$5.8^{+1.9}_{-1.1}$	10.1 ± 0.05	$1.9^{+0.4}_{-0.6}$
z3-D	0.9 – 1.3	1.01	–25.0 – –20.0	100	$7.6^{+3.2}_{-1.9}$	11.2 ± 0.07	$1.6^{+0.4}_{-0.5}$
z2-B	0.6 – 0.9	0.79	–30.0 – –25.0	113	$6.3^{+2.4}_{-1.5}$	13.9 ± 0.10	$2.3^{+0.4}_{-0.6}$
z3-B	0.9 – 1.3	1.06	–30.0 – –25.0	274	$5.1^{+2.7}_{-1.5}$	11.1 ± 0.04	$1.4^{+0.4}_{-0.5}$
z4-B	1.3 – 1.8	1.54	–30.0 – –25.0	142	$11.1^{+6.1}_{-2.7}$	19.4 ± 0.07	$1.3^{+0.4}_{-0.6}$
z5-B	1.8 – 3.0	2.07	–30.0 – –25.0	109	< 13.1	14.4 ± 0.07	$0.49^{+0.19}_{-0.24}$
z1-D (IR)	0.3 – 0.6	0.46	–25.0 – –20.0	584	$6.8^{+1.9}_{-1.0}$	7.73 ± 0.05	$2.2^{+0.4}_{-0.6}$
z1-D (OPT)	0.3 – 0.6	0.46	–25.0 – –20.0	67	$3.0^{+1.5}_{-1.1}$	147.0 ± 0.67	$22.3^{+2.8}_{-4.6}$
z2-D (IR)	0.6 – 0.9	0.73	–25.0 – –20.0	374	$7.4^{+4.7}_{-2.1}$	3.50 ± 0.03	$0.56^{+0.22}_{-0.27}$
z2-D (OPT)	0.6 – 0.9	0.74	–25.0 – –20.0	46	$5.0^{+1.6}_{-1.0}$	63.5 ± 0.34	$12.7^{+1.8}_{-2.9}$

* average redshift

 † K-corrected absolute magnitude range ‡ number of AGNs $^\parallel$ correlation length, the quoted error contains systematic error due to uncertainty of ρ_0 and one sigma statistical error. § projected galaxy number density for background $^\#$ average galaxy number density at the AGN redshift

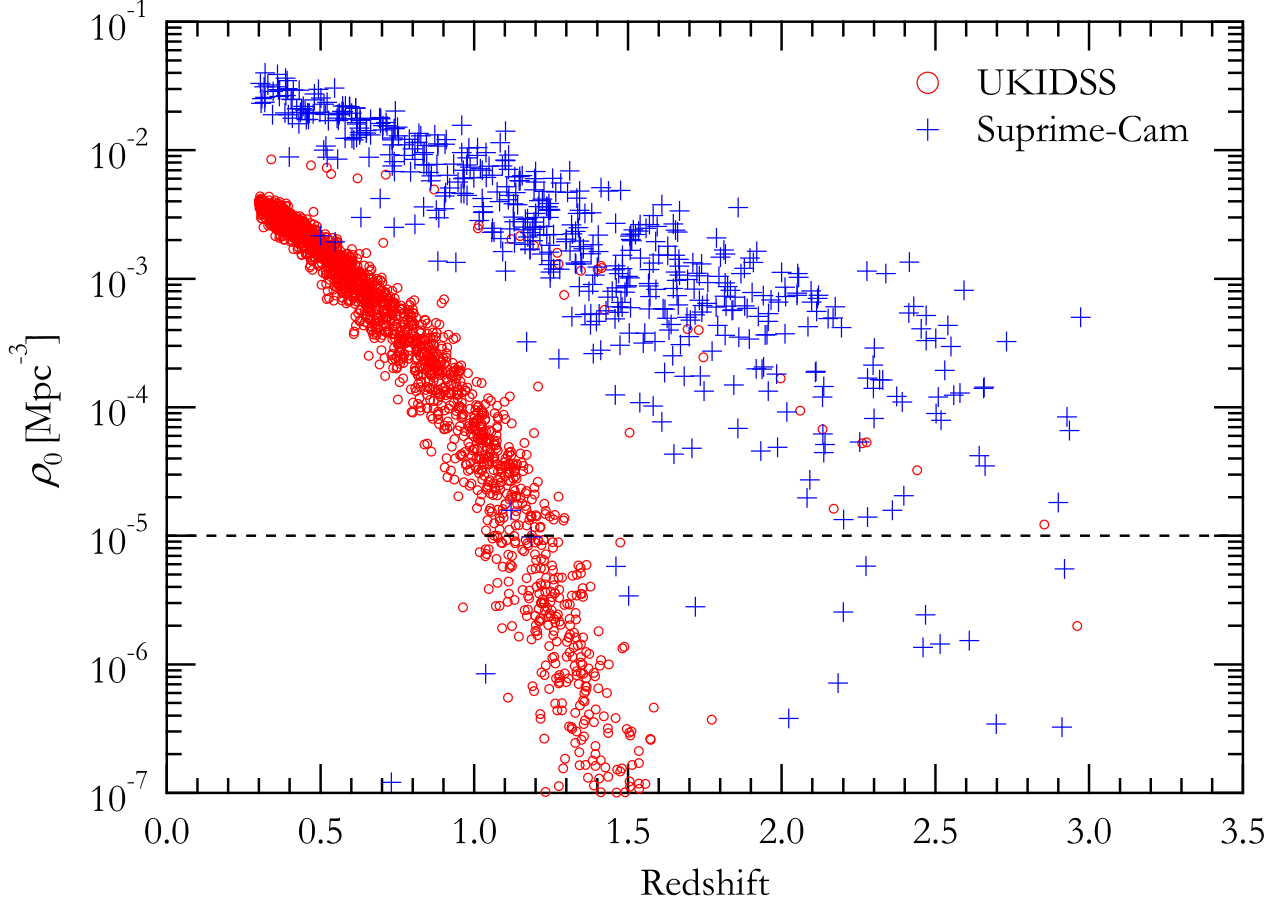


Fig. 1. The distribution of the average number density ρ_0 of detectable galaxies at the AGN redshift z . Data of $\rho_0 > 10^{-7} \text{ Mpc}^{-3}$ among the 2689 samples are plotted. The open circles and crosses represent AGN samples for which the galaxy sample is derived from the UKIDSS and the Suprime-Cam data, respectively. The horizontal dashed line represents the threshold for data selection.

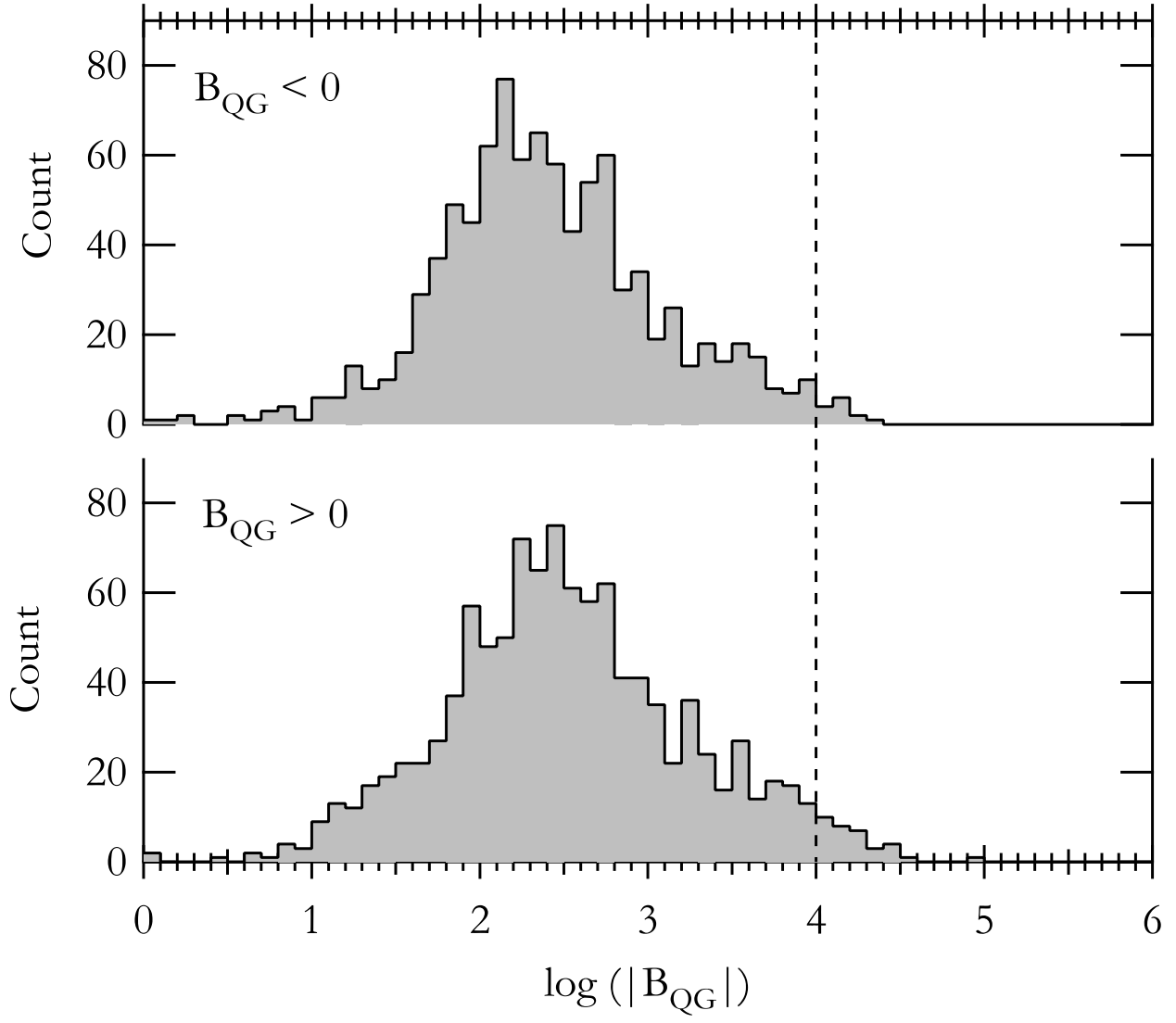


Fig. 2. The logarithmic distribution of clustering coefficient B_{QG} for 2023 samples which are selected with the criterion $\rho_0 > 10^{-5} \text{ Mpc}^{-3}$. The top panel is for negative B_{QG} and the bottom panel is for positive B_{QG} . The vertical dashed lines represent the upper limits for data selection.

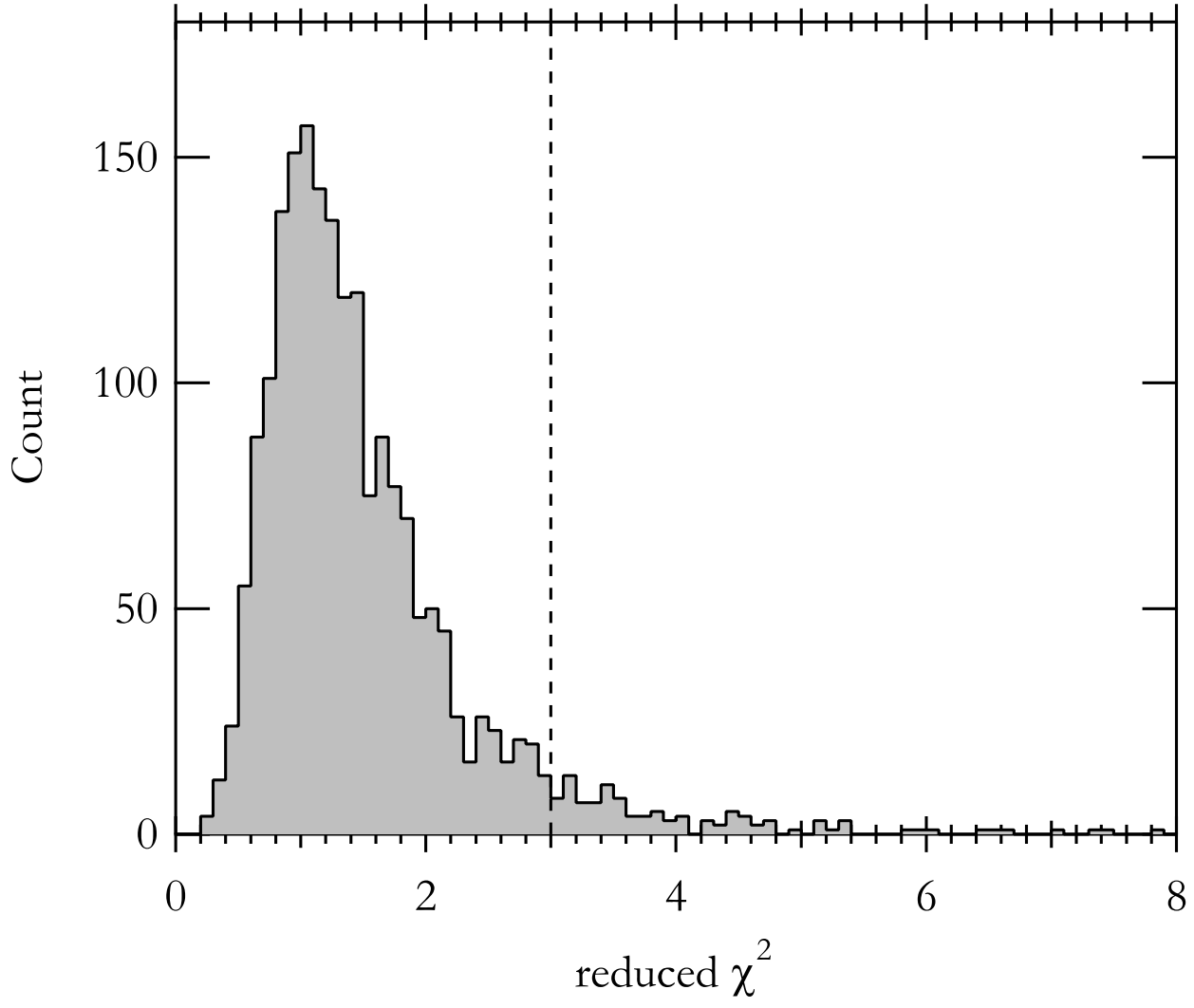


Fig. 3. The distribution of reduced χ^2 of number density at radial distance from 1 Mpc to $r_{\text{bg,min}}$ for 1976 AGN samples. The vertical dashed line represent the maximum value for sample selection.

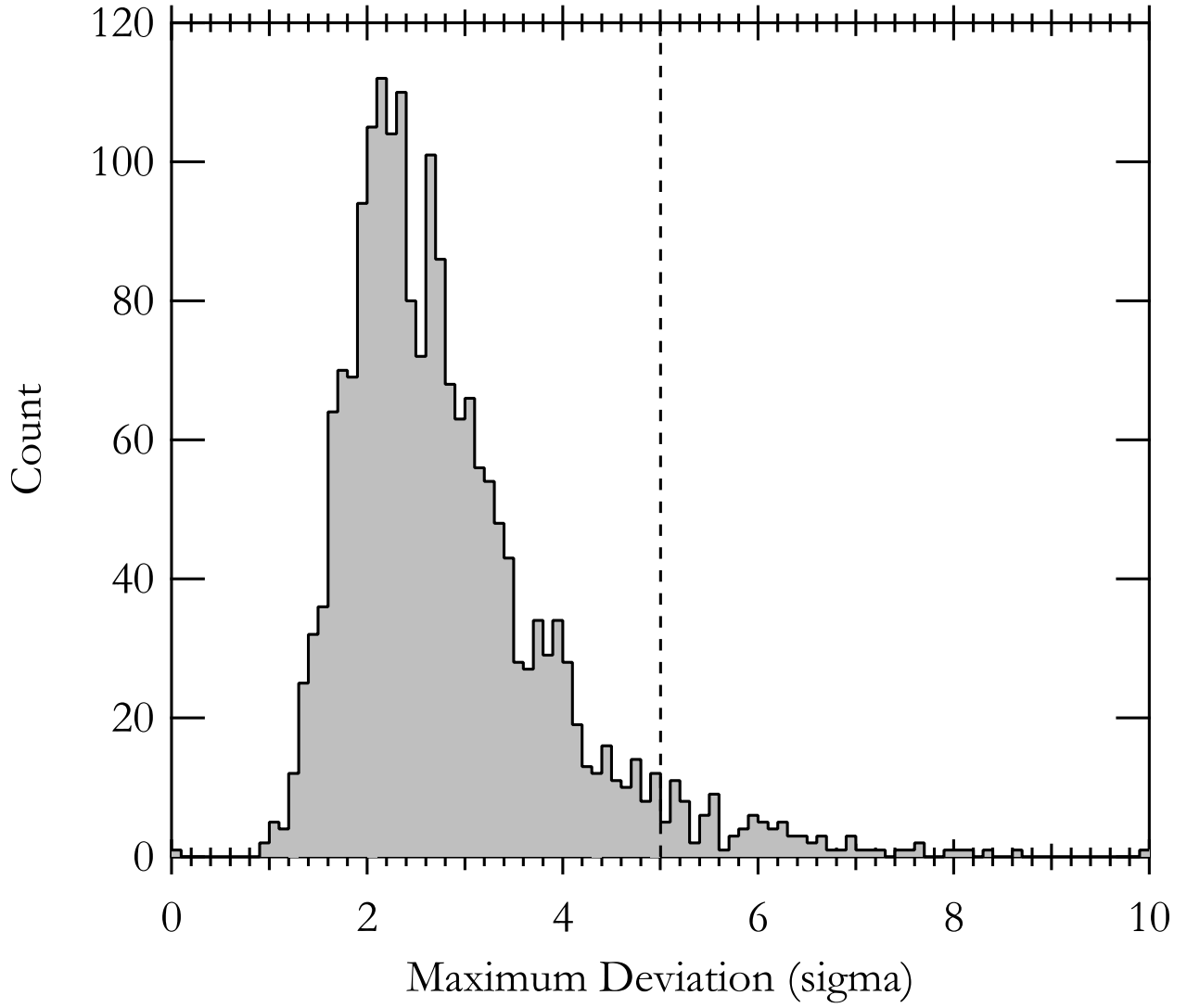


Fig. 4. The distribution of maximum deviation of number density measured in the unit of a standard deviation at radial distance from 1 Mpc to $r_{\text{bg,min}}$ for 1976 AGN samples. The vertical dashed line represent the maximum value for sample selection.

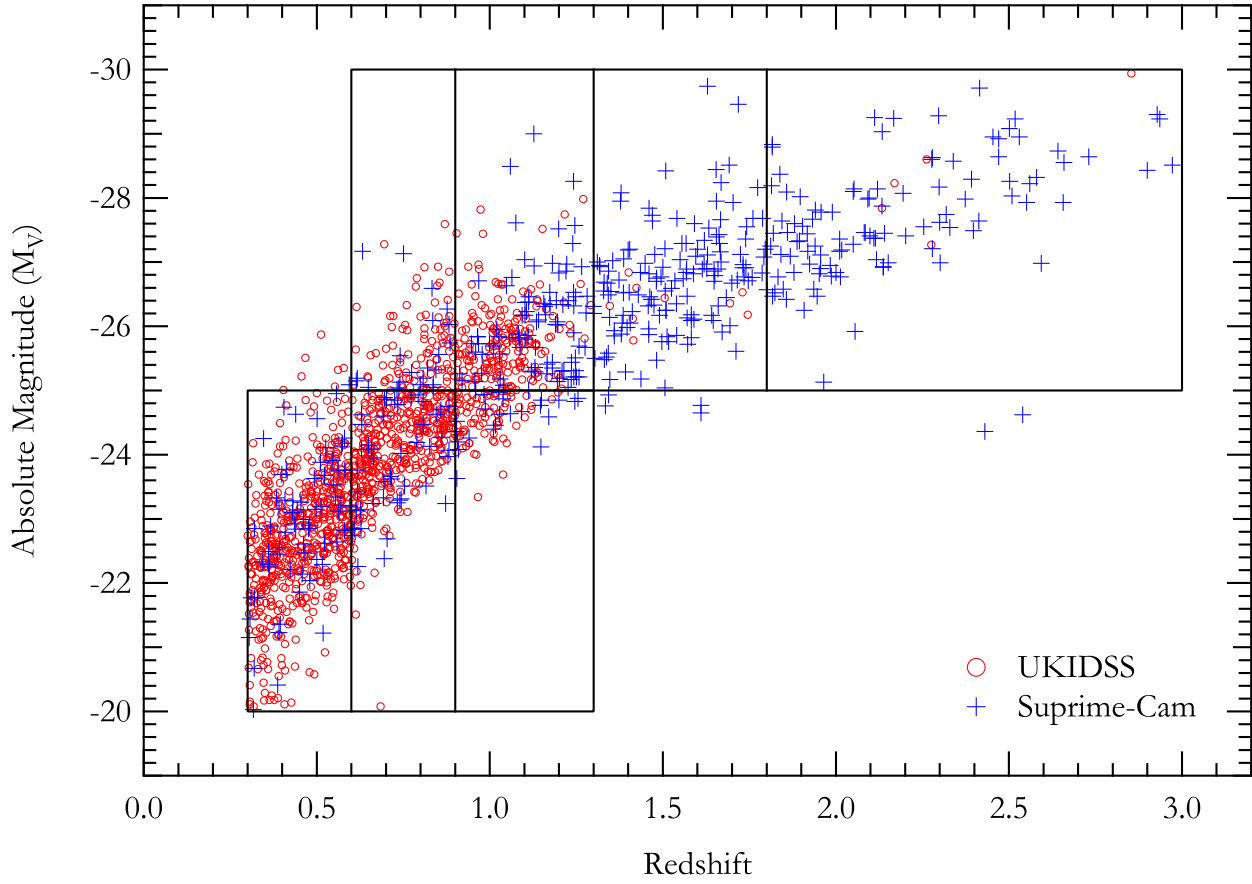


Fig. 5. K-corrected V band absolute magnitude vs redshift of the AGNs used in this work. Open circles represent AGN samples for which the galaxy sample is derived from the UKIDSS data, and the crosses represent AGN samples for which the galaxy sample is derived from the Suprime-Cam data.

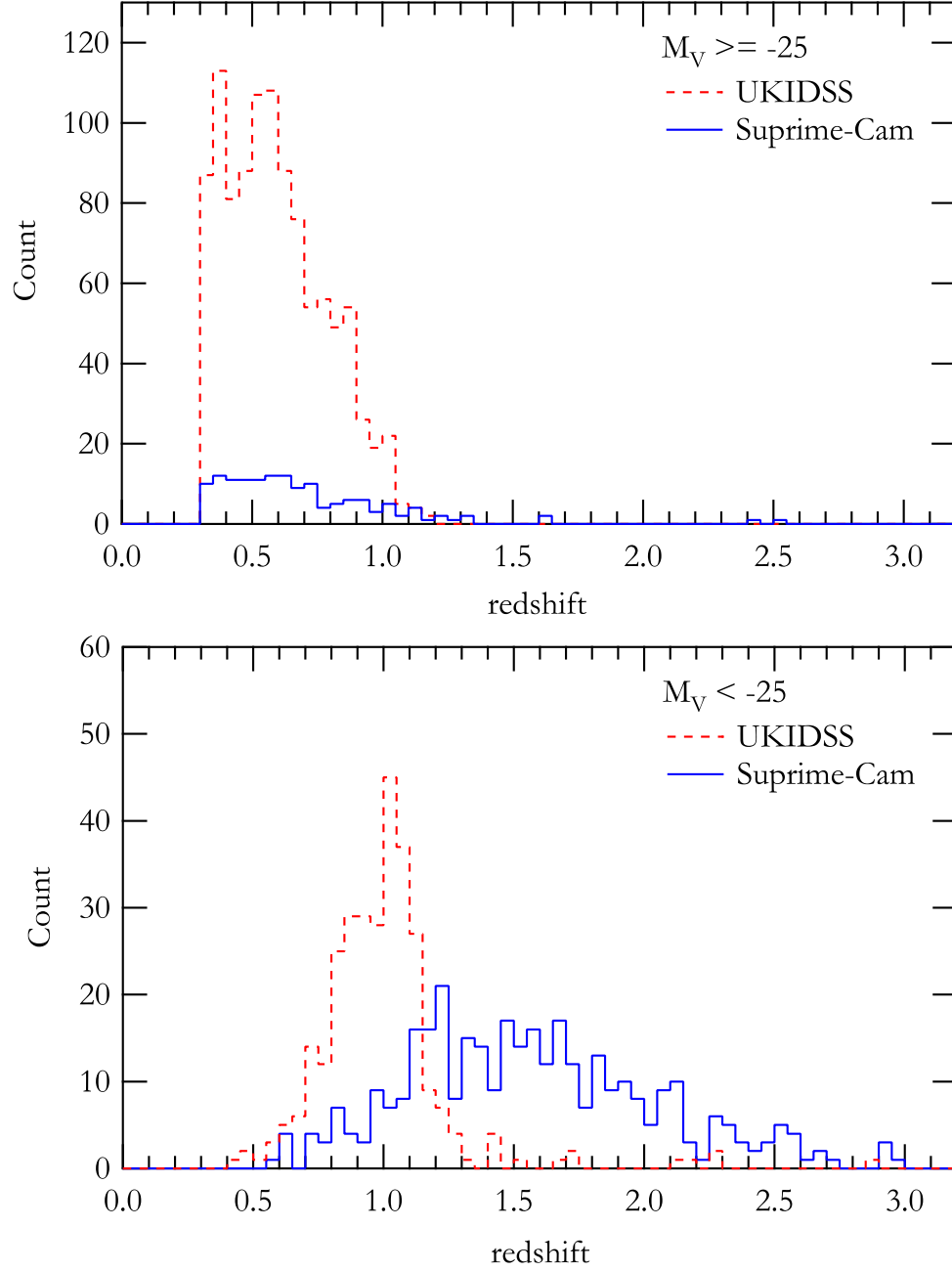


Fig. 6. Redshift distributions for dim AGN samples (top) and bright AGN samples (bottom). The dashed histogram represents AGN samples for which the galaxy sample is derived from the UKIDSS data, and the solid line histogram represents AGN samples for which the galaxy sample is derived from the Suprime-Cam data.

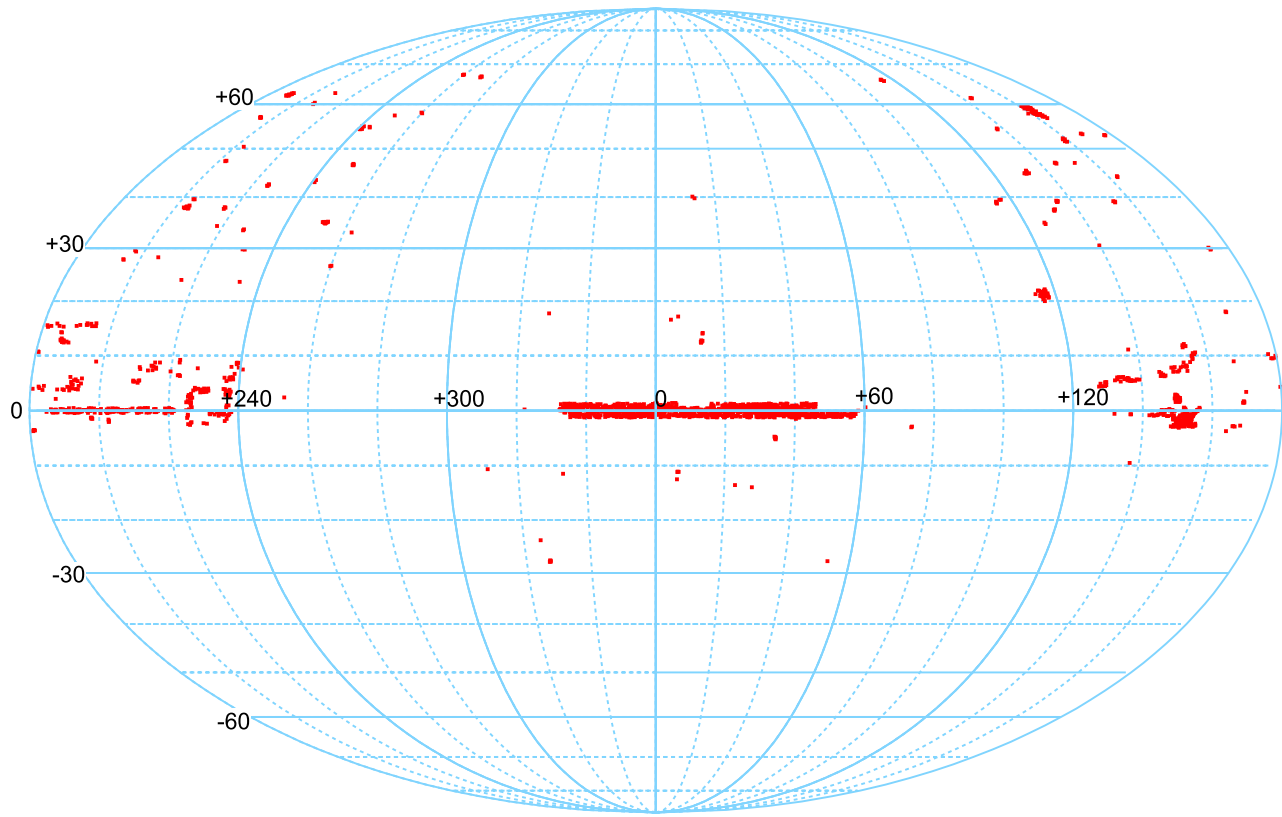


Fig. 7. The distribution of 1,809 AGNs analyzed in this work. The coordinates are in equatorial.

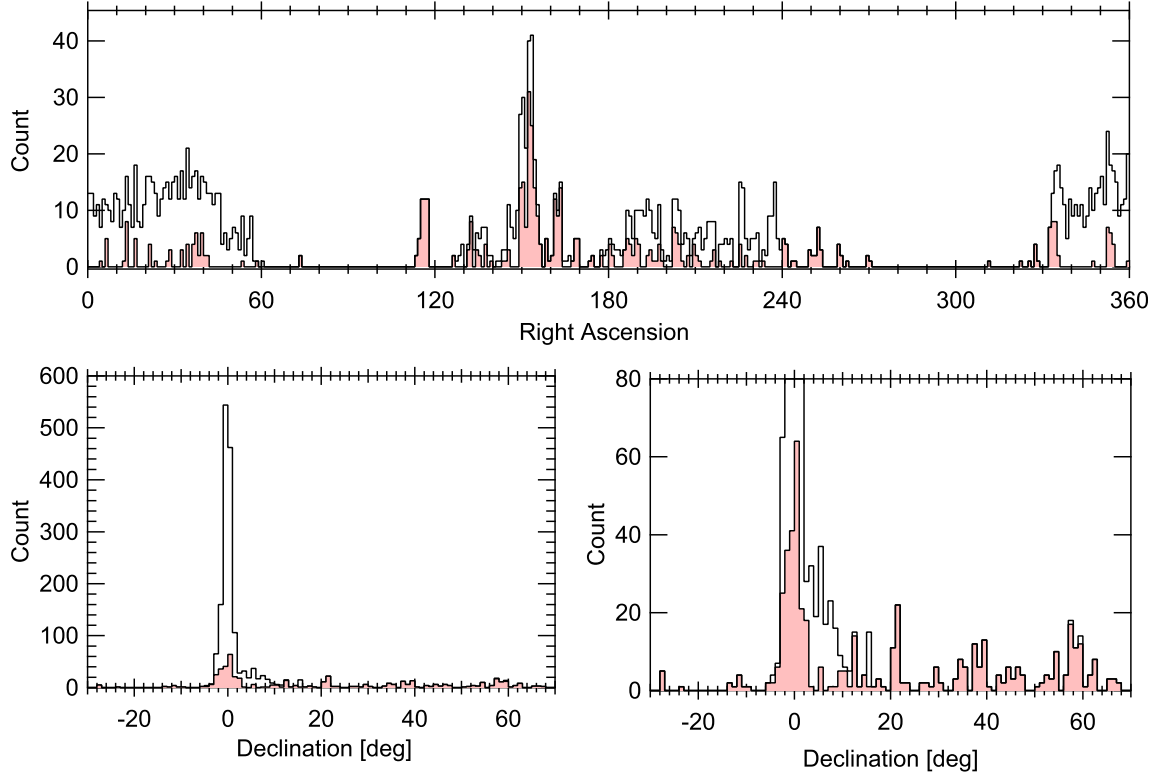


Fig. 8. The distribution of AGN coordinates. The top panel is for the right ascension of AGN, the left bottom panel is for the declination, and the right bottom panel is a close up of the declination distribution, showing detailed distribution of low counts. Open histogram is for all the AGNs and the shaded histogram is for AGNs for which the Suprime-Cam data was used.

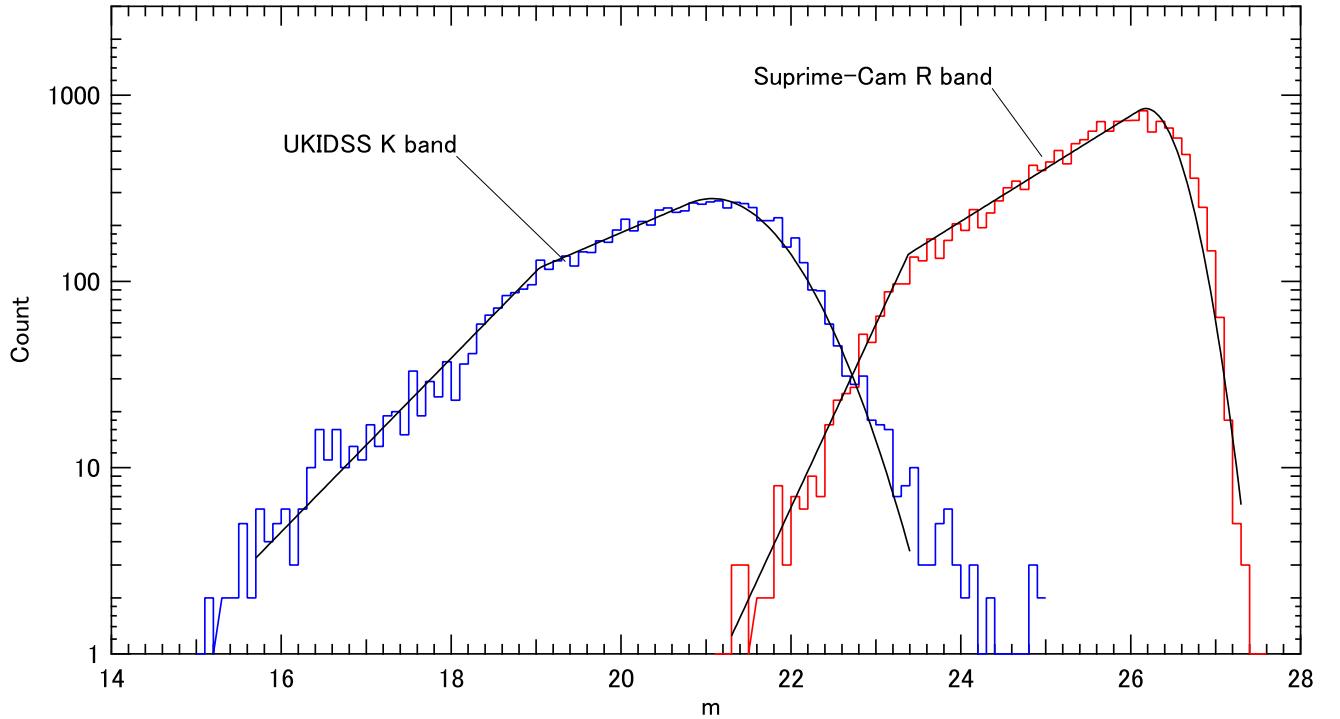


Fig. 9. Examples of the observed magnitude distributions and their model functions. The left histogram shows the UKIDSS K-band data and the right one shows the Suprime-Cam R-band data.

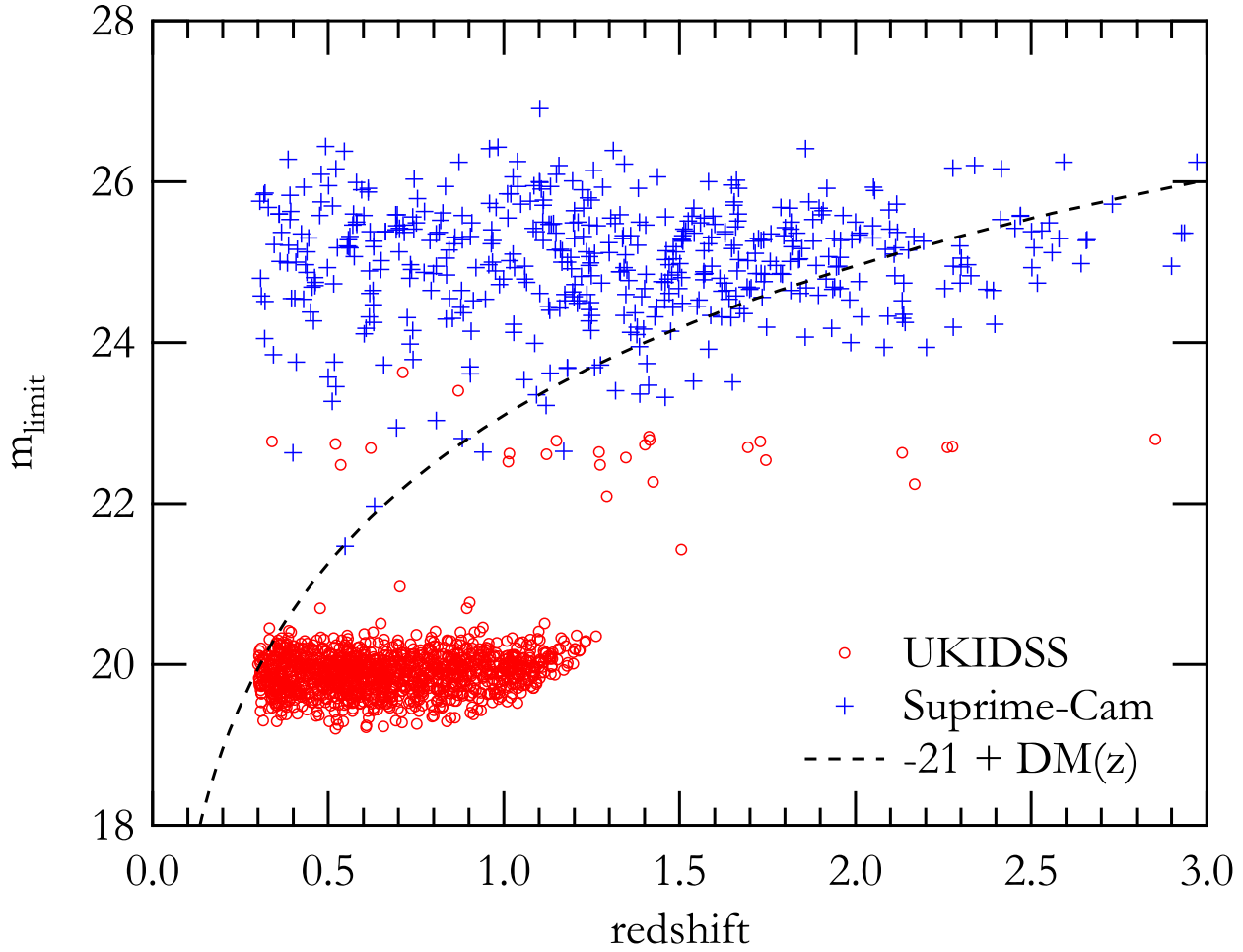


Fig. 10. Distribution of m_{limit} and AGN redshift. The open circles correspond to AGNs for which the galaxy sample is derived from the UKIDSS data, and the crosses correspond to AGNs for which the galaxy sample is derived from the Suprime-Cam data. The dashed line represents apparent magnitude which corresponds to absolute magnitude of -21 at the redshift.

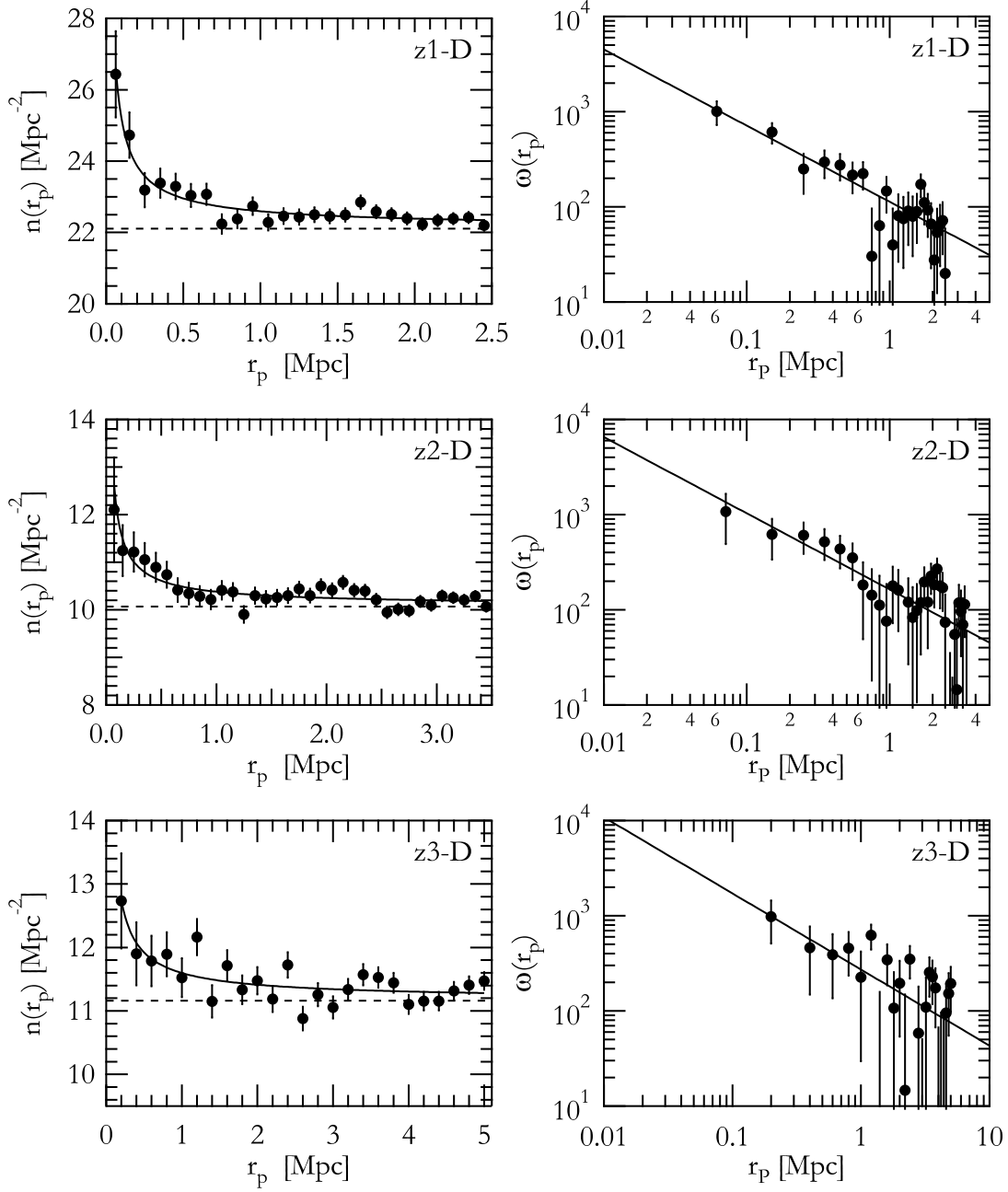


Fig. 11. The distributions of number density of detected sources and the projected correlation functions for dim AGN groups. The left panels show the averaged galaxy number density as a function of projected distance from the AGN, and the corresponding projected correlation functions are shown in the right panels. The dashed lines in the left panels represent fitting parameter n_{bg} . The solid lines represent the model function fitted to the observational data.

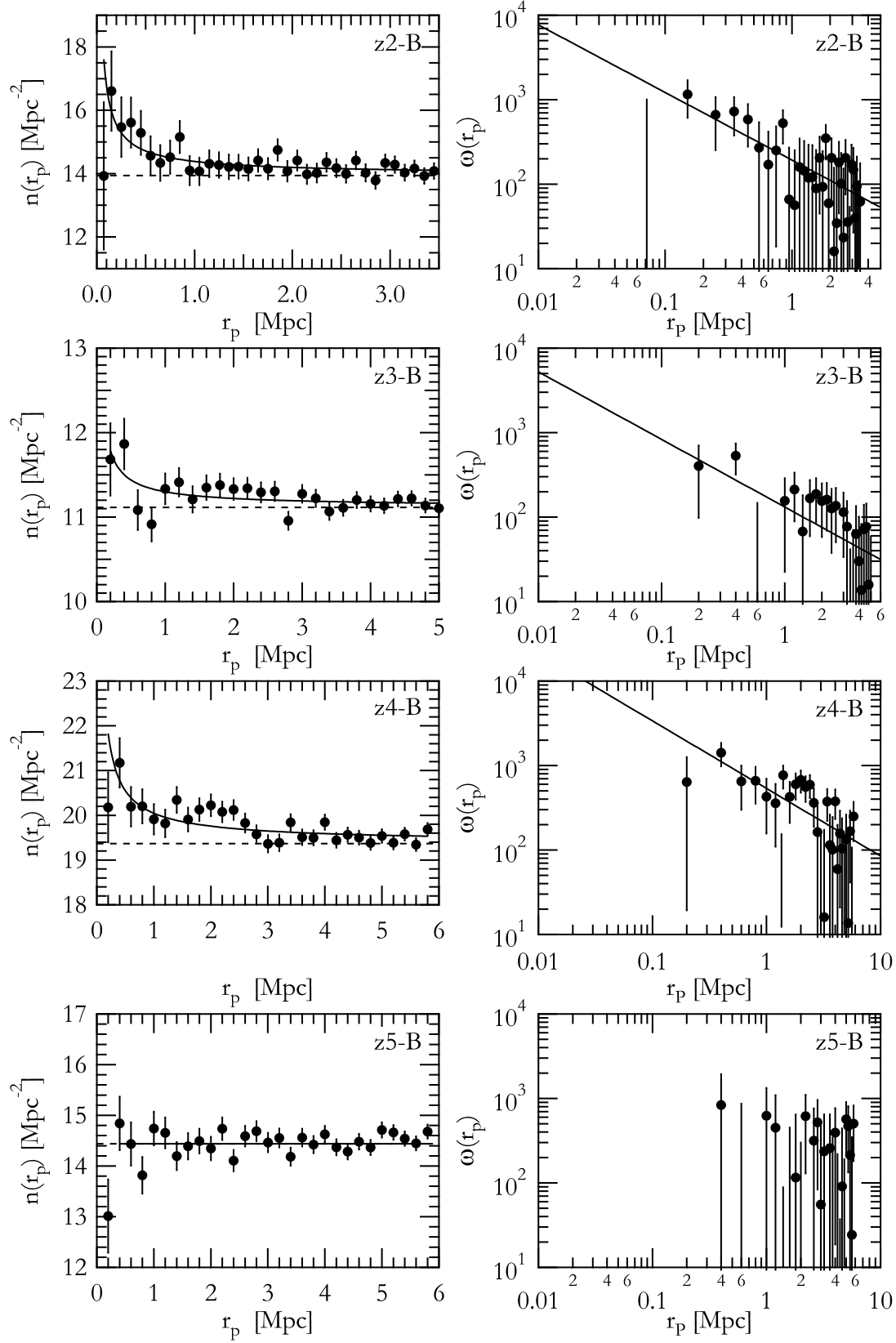


Fig. 12. The distributions of number density of detected sources and the projected correlation functions for bright AGN groups. The other explanation of this figure is the same as figure 11.

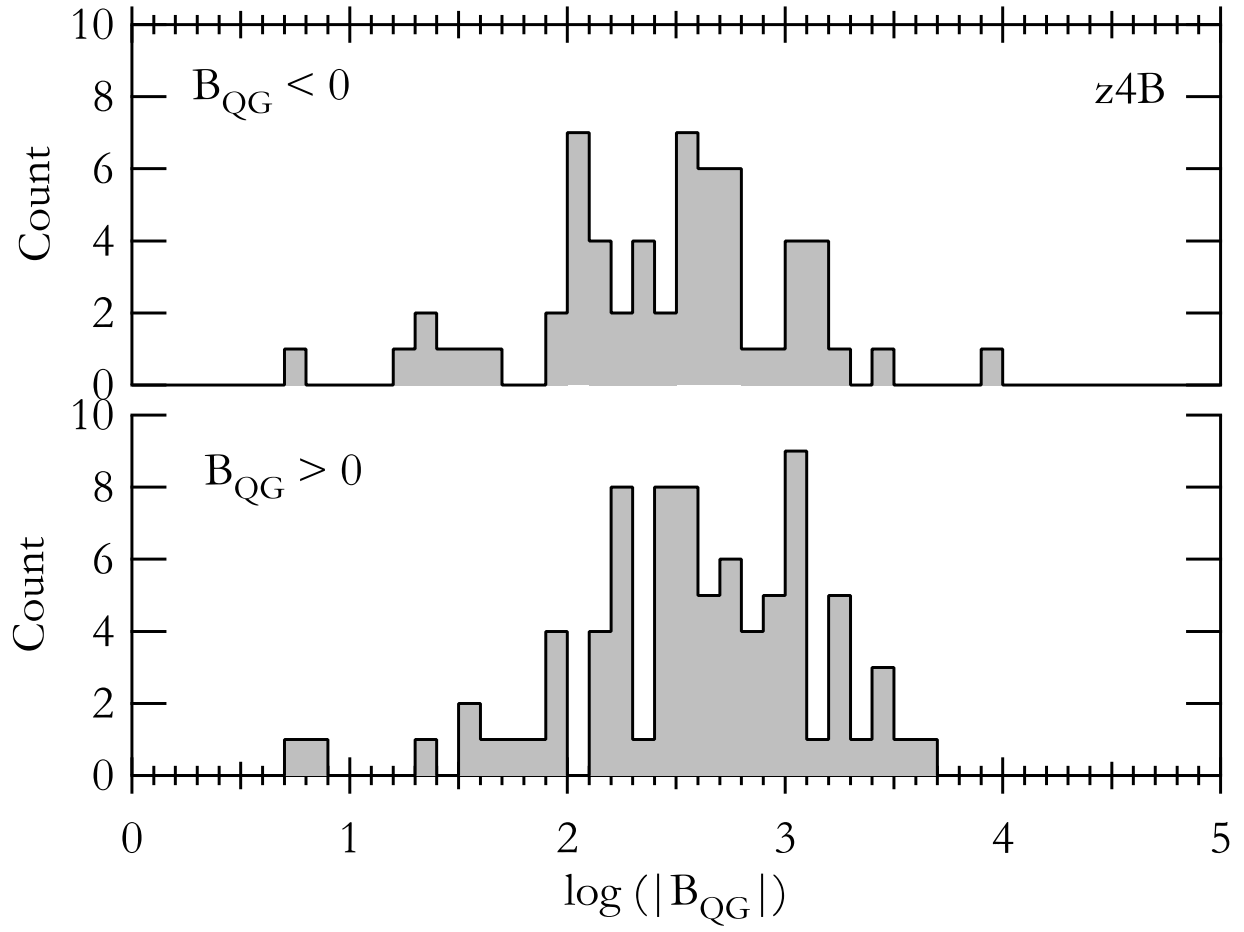


Fig. 13. The logarithmic distribution of clustering coefficient B_{QG} for 142 z4-B samples. The top panel is for negative B_{QG} and the bottom panel is for positive B_{QG} .

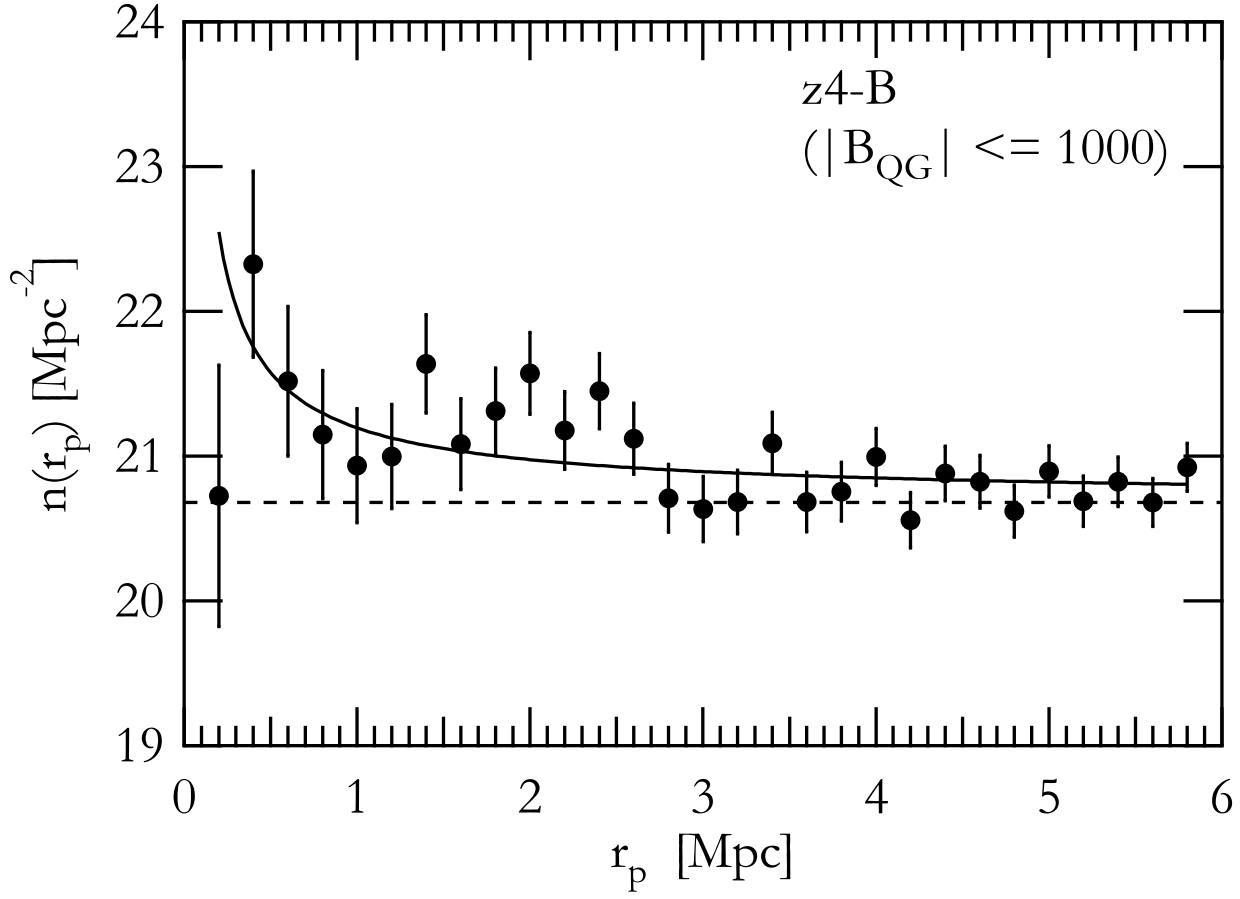


Fig. 14. Averaged number density around z4-B AGNs which satisfy the condition $|B_{QG}| \leq 1000$.

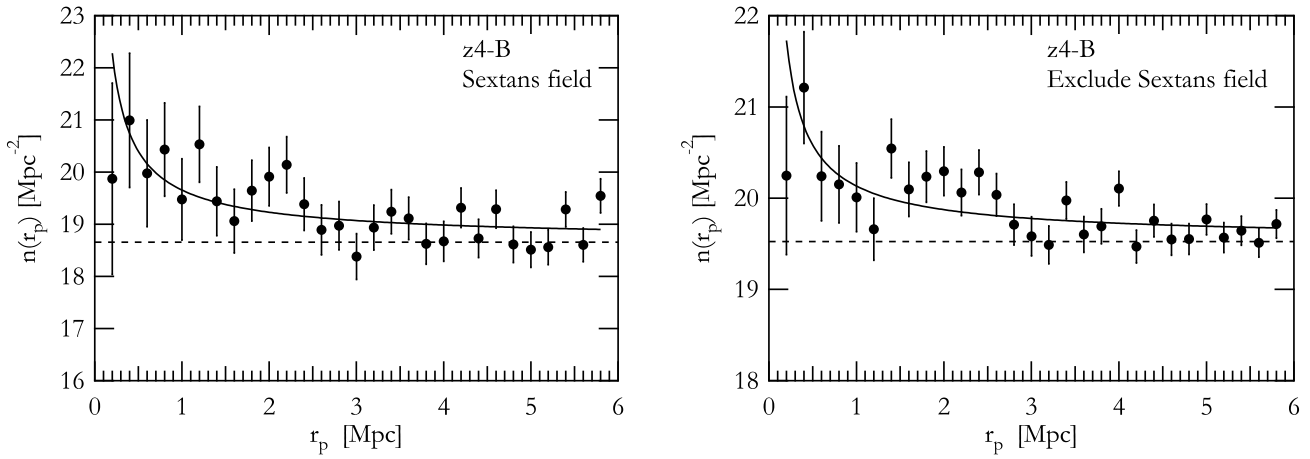


Fig. 15. Averaged number density around z4-B AGNs not located in the Sextans field (left) and AGNs located in the Sextans field (right).

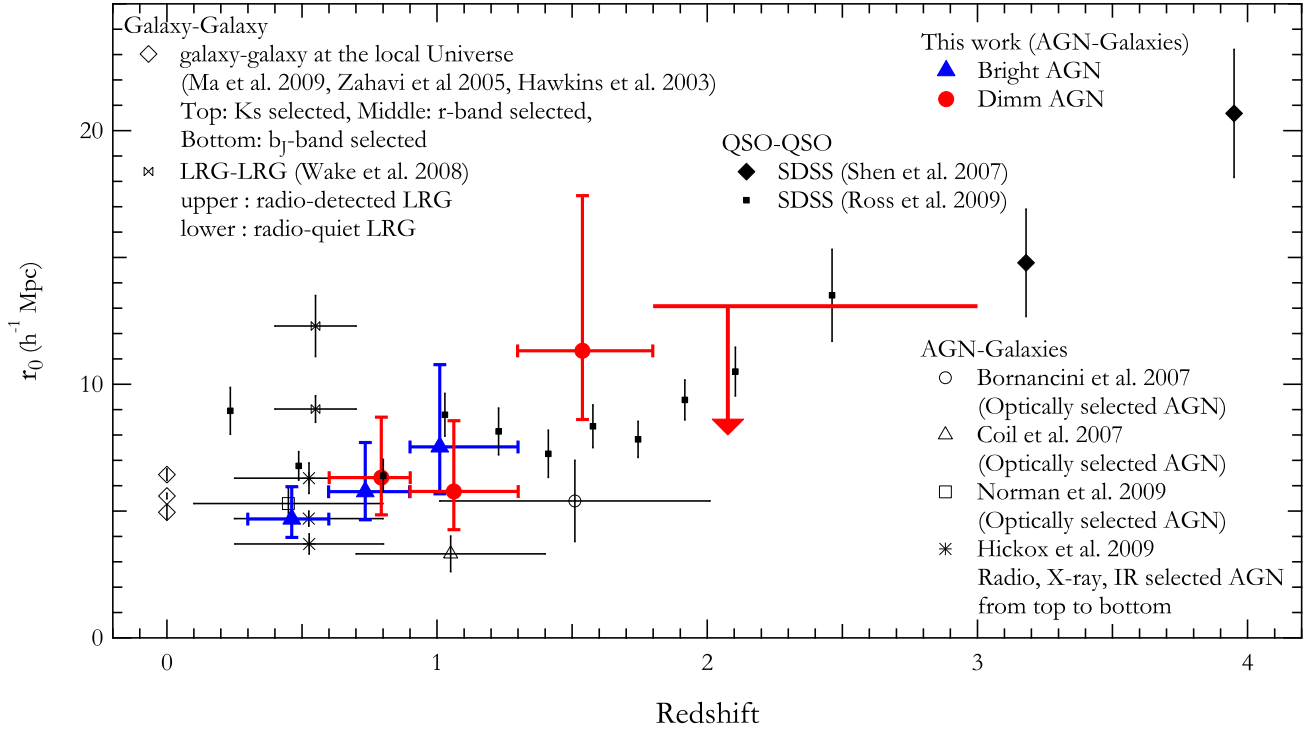


Fig. 16. Measured correlation length, r_0 , as a function of redshift. The error bars of our results indicate sum of the systematic error estimated from uncertainty of ρ_0 and the statistical error of one sigma. The closed triangles represent the result for dim AGN groups, and the closed circles represent the result for bright AGN groups. The result for z5-B are shown with the upper limits.

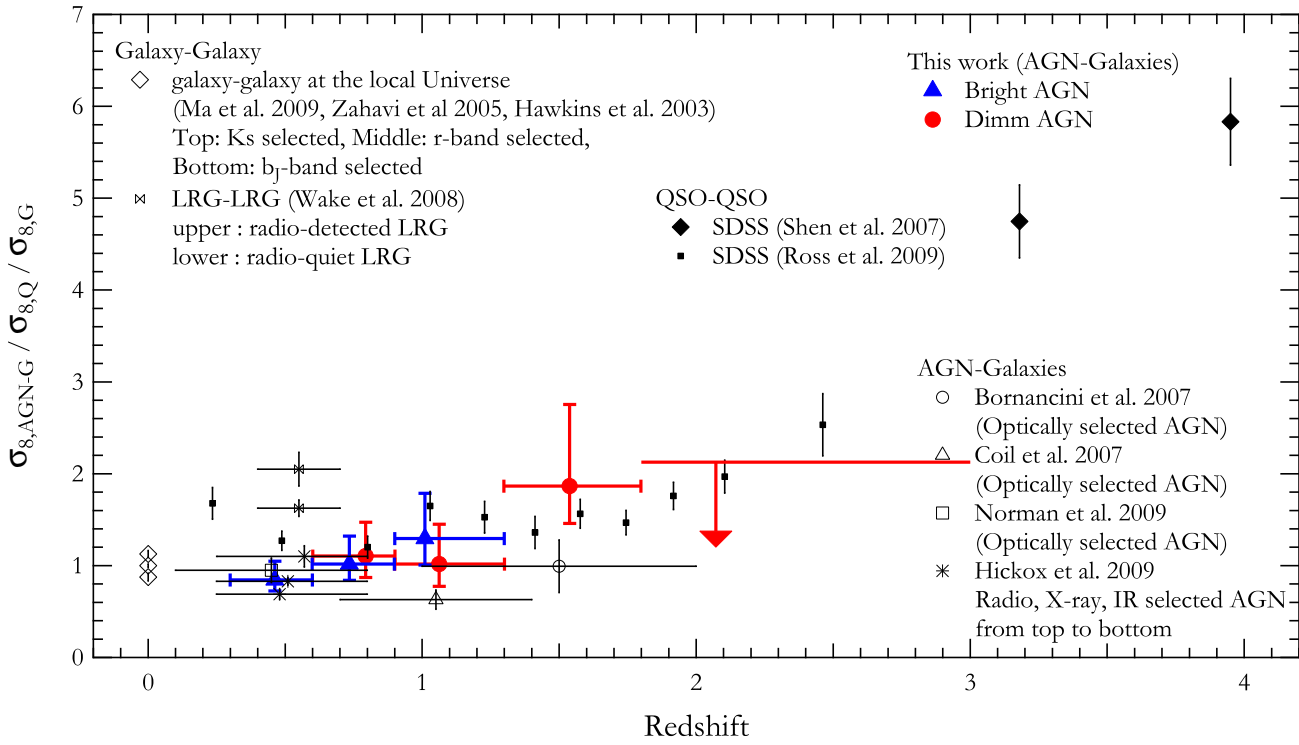


Fig. 17. The σ_8 of the galaxies around AGNs ($\sigma_{8,AGN-G}$), QSOs ($\sigma_{8,Q}$), and galaxies ($\sigma_{8,G}$) are shown as a function of redshift. The error bars of our results indicate sum of the systematic error estimated from uncertainty of ρ_0 and the statistical error of one sigma.

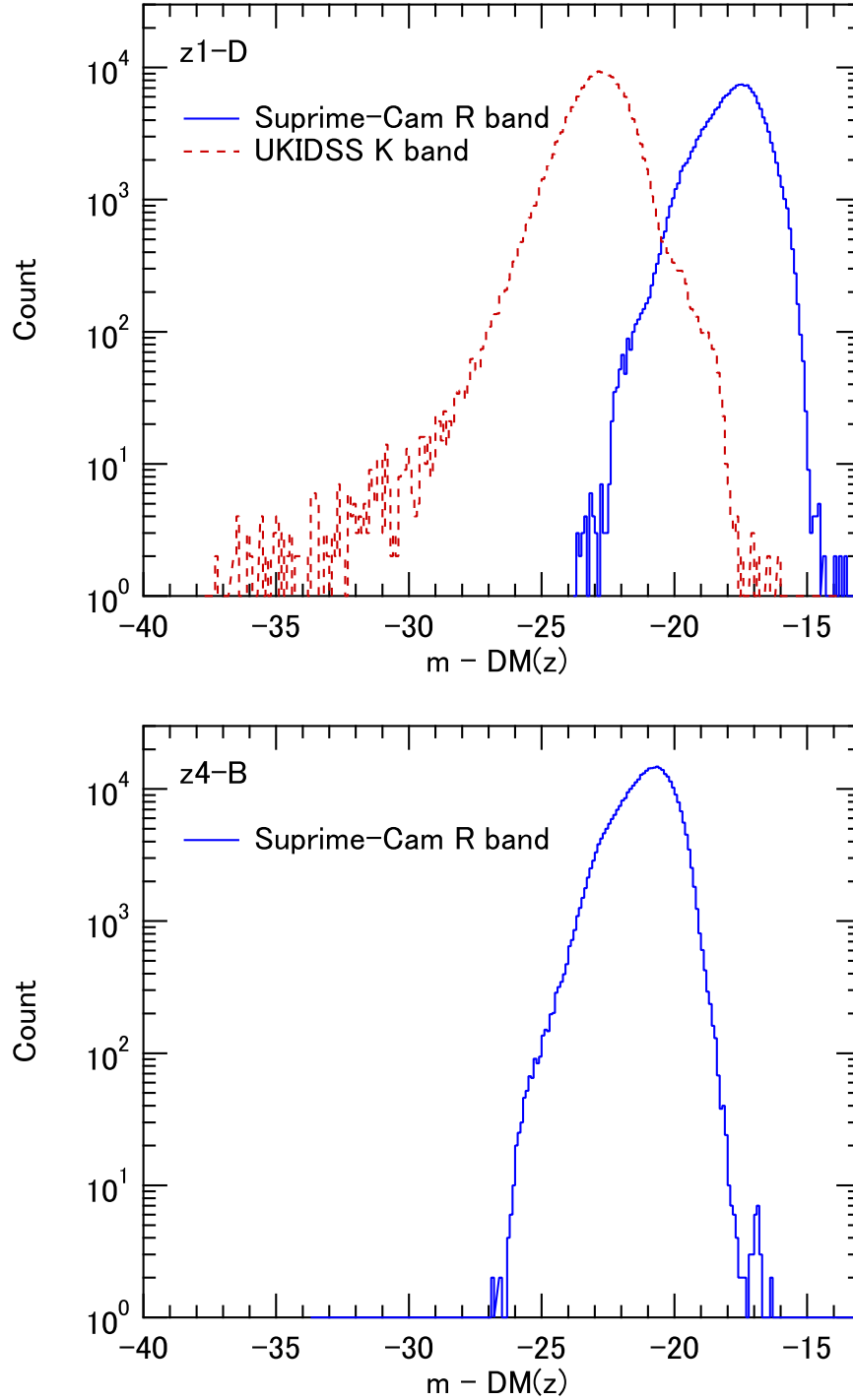


Fig. 18. The distribution of $m - DM(z)$, where m is an apparent magnitude of detected objects, and $DM(z)$ is a distance modulus corresponding to the AGN redshift. The top panel shows the distribution for z1-D galaxy samples observed with Suprime-Cam in R band (solid line) and in UKIDSS K band (dashed line). The bottom panel shows the distribution for z4-B galaxy samples observed with Suprime-Cam in R band.

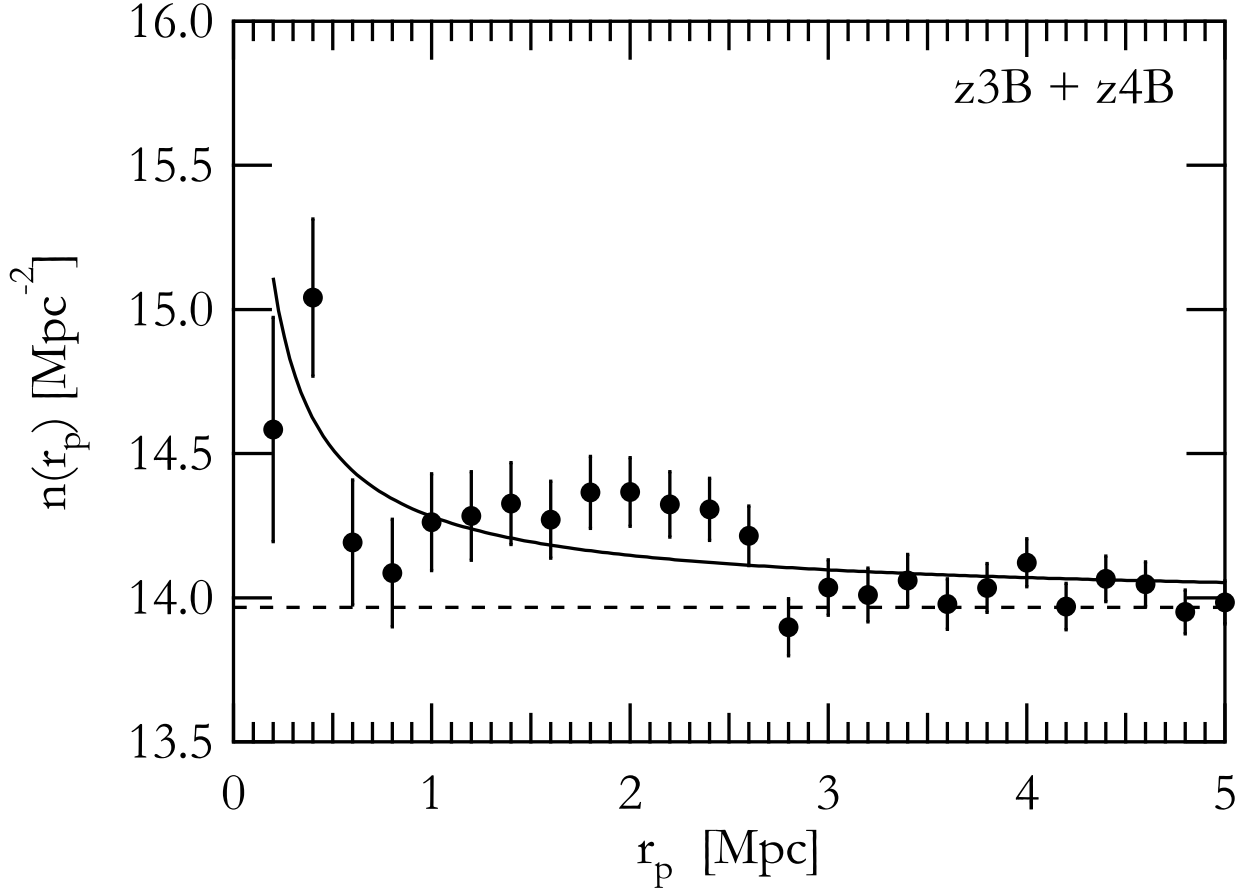


Fig. 19. Averaged number density around z3-B and z4-B AGNs.

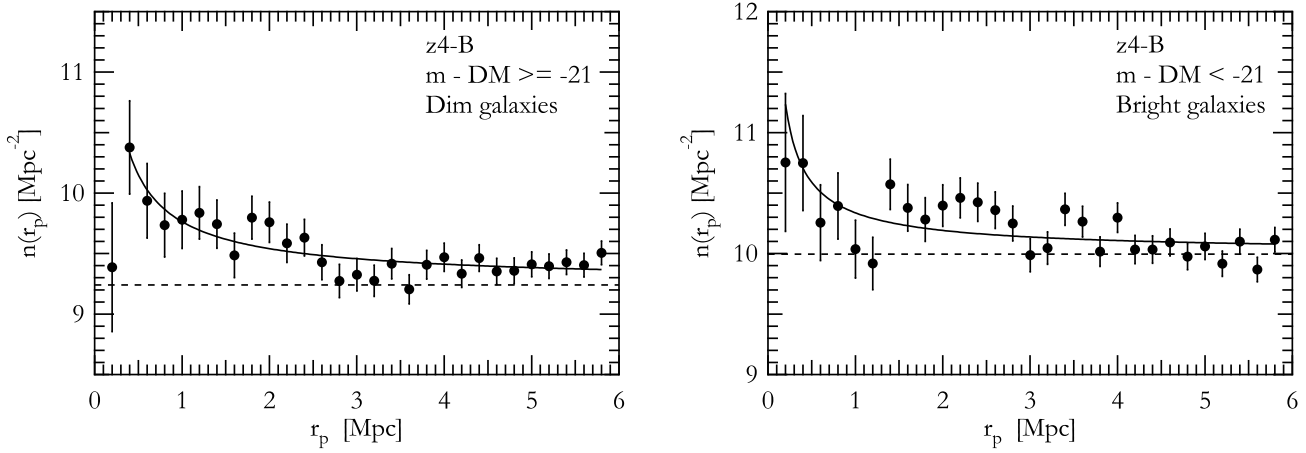


Fig. 20. Averaged number density of dim sources ($m \geq -21 + DM$) (left panels) and of bright sources ($m < -21 + DM$) (right panels) around z4-B AGNs, where DM represents a distance modulus corresponding to AGN redshift. The solid lines represent model function of equation (13) fitted to the observation data. The fit was done for distance range of 0.1–2.0 Mpc for the case of dim sources, while 0.0–2.0 Mpc for bright sources. The horizontal lines represent the fitting parameter n_{bg} .